AD-A065 102 DAVID W TAYLOR NAVAL SHIP RESEARCH AND DEVELOPMENT CE--ETC F/G 13/10
PERFORMANCE OF A TAP-2 HYDROFOIL.(U)
JUN 78 P LAFRANCE
UNCLASSIFIED DTNSRDC/SPD-0843-01 NL

1 OF 2
ADA
065102

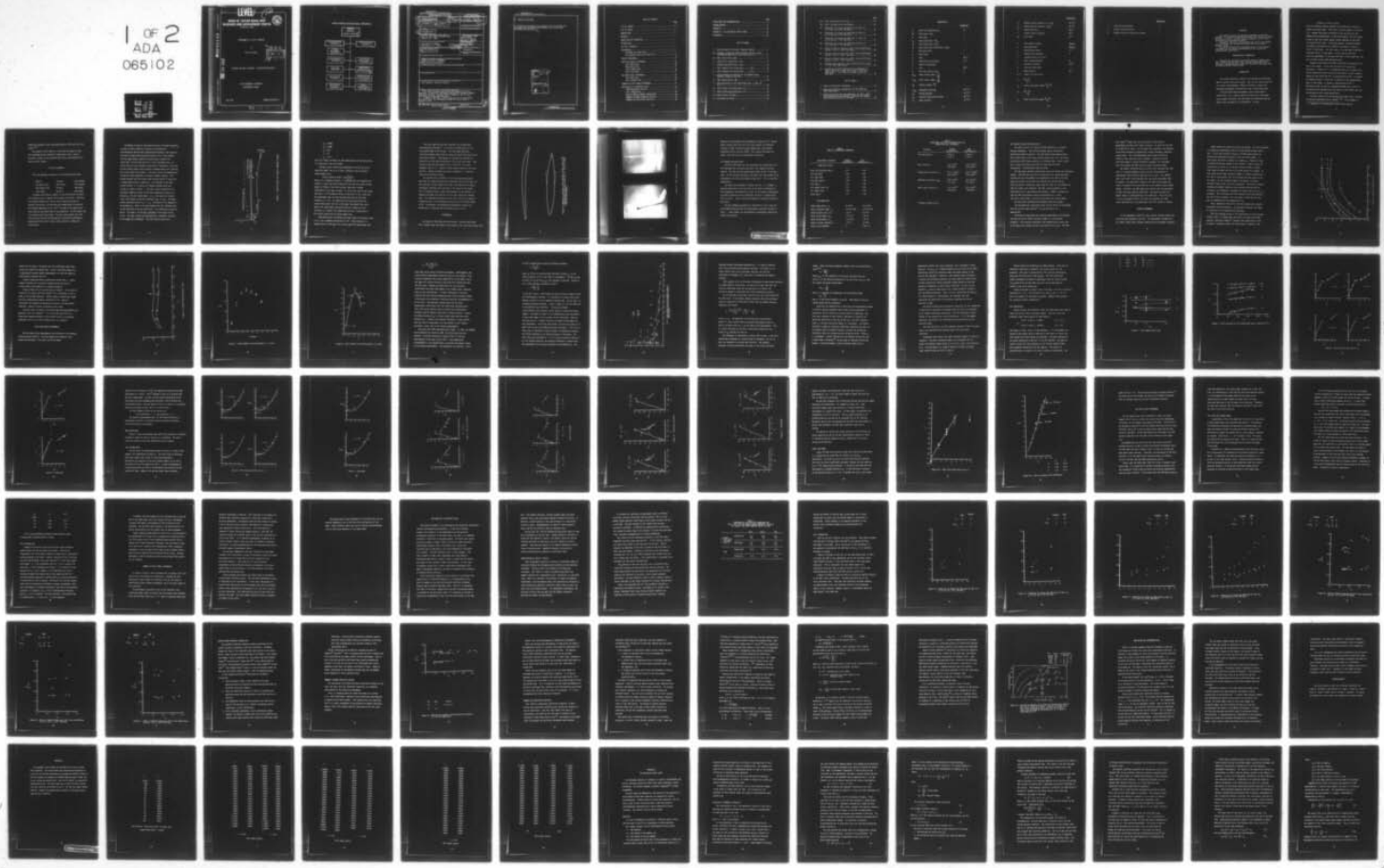

LEVEL II

DAVID W. TAYLOR NAVAL SHIP RESEARCH AND DEVELOPMENT CENTER

Bethesda, Md. 20084

PERFORMANCE OF A TAP-2 HYDROFOIL

by

Pierre Lafrance

APPROVED FOR PUBLIC RELEASE: DISTRIBUTION UNLIMITED

SHIP PERFORMANCE DEPARTMENT

DEPARTMENTAL REPORT

June 1978

DTNSRDC/SPD-0843-01

MAJOR DTNSRDC ORGANIZATIONAL COMPONENTS

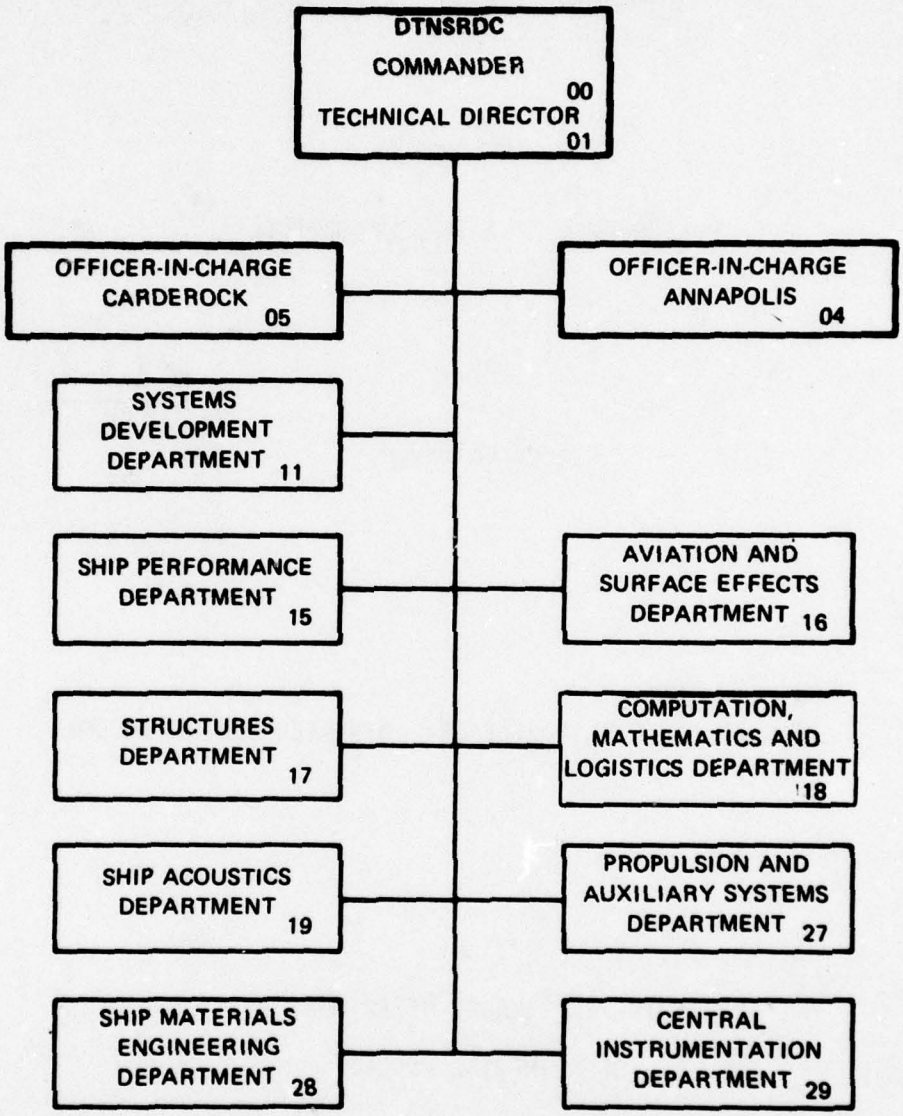

UNCLASSIFIED

SECURITY CLASSIFICATION OF THIS PAGE (When Date Entered)

REPORT DOCUMENTATION PAGE

READ INSTRUCTIONS BEFORE COMPLETING FORM

(14) 1. REPORT NUMBER: DTNSRDC/SPD-0843-01

2. GOVT ACCESSION NO. (19) Departmental Rept.

3. RECIPIENT'S CATALOG NUMBER

(6) 4. TITLE (and Subtitle): PERFORMANCE OF A TAP-2 HYDROFOIL

5. TYPE OF REPORT & PERIOD COVERED

6. PERFORMING ORG. REPORT NUMBER

(10) 7. AUTHOR(s): Pierre Lafrance

8. CONTRACT OR GRANT NUMBER(s)

9. PERFORMING ORGANIZATION NAME AND ADDRESS
David W. Taylor Naval Ship R&D Center
Bethesda, MD 20084

10. PROGRAM ELEMENT, PROJECT, TASK AREA & WORK UNIT NUMBERS
Element 62543N
Task Area ZF 4342100
Work Unit 1-1500-102

11. CONTROLLING OFFICE NAME AND ADDRESS
Naval Material Command
Washington, D.C. 20380

(11) 12. REPORT DATE: June 1978

(12) 102p. 13. NUMBER OF PAGES: 105

14. MONITORING AGENCY NAME & ADDRESS (if different from Controlling Office)
(16) F43421

15. SECURITY CLASS. (of this report): UNCLASSIFIED

15a. DECLASSIFICATION/DOWNGRADING SCHEDULE

16. DISTRIBUTION STATEMENT (of this Report)

APPROVED FOR PUBLIC RELEASE; DISTRIBUTION UNLIMITED

(17) ZF4342100

17. DISTRIBUTION STATEMENT (of the abstract entered in Block 20, if different from Report)

18. SUPPLEMENTARY NOTES

19. KEY WORDS (Continue on reverse side if necessary and identify by block number)
TAP-2 Hydrofoil, Strut-Foil System

20. ABSTRACT (Continue on reverse side if necessary and identify by block number)

This report discusses the measured performance of the TAP-2 hydrofoil, a "mixed foil" designed to operate fully wetted at takeoff (35 knots) and which, through a change in geometry, can fly fully ventilated at cruise speed (60 knots).

At takeoff, TAP-2 has a lift-to-drag ratio of 13 at the design lift coefficient; the corresponding figure for cruise speed is between 7 and 8.

CONF

DD FORM 1 JAN 73 1473 EDITION OF 1 NOV 65 IS OBSOLETE
S/N 0102-LF-014-6601

UNCLASSIFIED

SECURITY CLASSIFICATION OF THIS PAGE (When Date Entered)

389694

20. Abstract (Continued)

Predictive extrapolation to prototype scale is discussed and contrasted with our present understanding of the scaling laws associated with ventilation.

TABLE OF CONTENTS

LIST OF FIGURES

LIST OF TABLES

NOMENCLATURE

		Dimensions
A	Total foil planform area	L^2
AR	Foil aspect ratio	-
B	Strut span	L
C_D	Drag coefficient, D/Aq_∞	-
C_L	Lift coefficient, L/Aq_∞	-
C_s	Strut side force coefficient, $S/q_\infty hc'$	-
c	Foil mean chord	L
c'	Strut chord	L
D	Drag	MLT^{-2}
g	Gravitation acceleration	LT^{-2}
h	Depth of submergence	L
L	Lift	MLT^{-2}
ℓ	Foil span (tip to tip)	L
$N_{F,c}$	Chord Froude number, $\frac{V_o}{\sqrt{gc}}$	-
$N_{F,h}$	Depth Froude number, $\frac{V_o}{\sqrt{gh}}$	-
N_R	Reynolds number, $\frac{V_o x}{\nu}$	-
p_{atm}	Atmospheric pressure	$ML^{-1}T^{-2}$
p_c	Cavity pressure	$ML^{-1}T^{-2}$
p_o	Pressure above water surface	$ML^{-1}T^{-2}$
p_v	Vapor pressure	$ML^{-1}T^{-2}$

		Dimensions
p_∞	Ambient static pressure = $p_o + \rho gh$	$ML^{-1}T^{-2}$
q_∞	Ambient dynamic pressure, $\frac{1}{2}\rho V_o^2$	$ML^{-1}T^{-2}$
S	Strut side force	MLT^{-2}
T	Surface tension constant	MT^{-2}
V_o	Foil speed	LT^{-1}
α	Foil angle of attack	degrees
β	Strut yaw angle	degrees
ζ	Amplification factor	T^{-1}
η	Surface wave amplitude	L
λ	Lockheed model scale ratio	-
μ	Mass scaling parameter	M
ν	Kinematic viscosity	L^2T^{-1}
ξ	Pressure coefficient	-
ρ	Water density	ML^{-3}
Σ, Σ'	Labels for fluid flows	-
σ	$\frac{p_o - p_v}{q_\infty}$	-
σ_c	Cavity cavitation number $\frac{p_\infty - p_c}{q_\infty}$	-
σ_s	$\frac{p_o - p_c}{q_\infty}$	-
σ_v	Vapor cavitation number $\frac{p_\infty - p_v}{q_\infty}$	-

		Dimensions
τ	Time scaling parameter	T
χ	Length scaling parameter	L
Ω	Denotes a point on the cavity surface	-

ABSTRACT

This report discusses the measured performance of the TAP-2 hydrofoil, a "mixed foil" designed to operate fully wetted at takeoff (35 knots) and which, through a change in geometry, can fly fully ventilated at cruise speed (60 knots).

At takeoff, TAP-2 has a lift-to-drag ratio of 13 at the design lift coefficient; the corresponding figure for cruise speed is between 7 and 8.

Predictive extrapolation to prototype scale is discussed and contrasted with our present understanding of the scaling laws associated with ventilation.

ADMINISTRATIVE INFORMATION

This work was authorized by the Naval Material Command (Code 08T), funded under the Ships, Subs, and Boat Program Task Area ZF 43-421, and administered by the Ship Performance Department High Performance Vehicle Program (1507).

INTRODUCTION

This report presents an analysis of experimental observations made on the TAP-2 strut-foil system. TAP-2 is the latest mixed foil in a series of developmental efforts to produce a system with acceptable performance characteristics over a wide speed range.

The wide speed range requirements raise serious design difficulties. For a takeoff speed of 35 knots and a high speed cruise speed of 60 knots, the high speed lift coefficient must be smaller than the takeoff lift coefficient. In fact,

$$C_L(60 \text{ kt}) = 0.34\ C_L\ (35 \text{ kt}),$$

with the difference between required lift coefficients increasing rapidly with speed range. TAP-2 uses a variable geometry to control lift. Another significant difficulty is that two distinct flow régimes must be accommodated. To facilitate takeoff, the foil should operate in the fully wetted régime, taking advantage of the large lift-to-drag (L/D) ratio. At 60 knots however, cavitation becomes unavoidable, and operation at a depth of one chord is likely to result in ventilation. For this reason, it was decided to maintain a ventilated cavity at high speeds. To this must be added the auxiliary requirements of low speed (45 knots) cruise capability, and short periods of high speed (80 knots) dash.

Research efforts were initiated to ascertain the feasibility of such a foil system. To this end, the mixed foil concept was introduced. A mixed foil is a streamlined hydrofoil equipped with a flap or other device which can be activated above a certain speed to change the flow around the foil to supercavitating flow. At takeoff and moderate speeds, a mixed foil is operated in the subcavitating mode; at high speeds, it becomes a supercavitating foil.[1*] Ventilation needs are met by a pseudoblunt-based strut, which is a streamlined strut equipped with side flaps or other devices that can be activated to form a base-vented strut.

The first mixed foil to be designed and tested, TAP-1, had poor lift-to-drag characteristics at takeoff.[1-4,7] In an attempt to

---

* A complete list of References can be found on page 93.

remedy this problem, a new system designated as TAP-2 was built and tested.[1,5-7]

The purpose of this report is to provide an analysis of the TAP-2 performance data reported in References 6 and 7, and to ascertain, insofar as the available data allow, the feasibility of the mixed foil concept.

THE TAP-2 HYDROFOIL

TAP-2 was designed to operate in the following speed range

takeoff	35 knots	fully wetted
low speed cruise	40-50 knots	fully wetted
high speed cruise	60 knots	ventilated
burst speed	80 knots	ventilated

To reduce craft drag at takeoff, it was decided that the TAP-2 foil should be able to takeoff fully wetted at 35 knots. Similarly, fully wetted operation at the low cruise speed should make it possible to achieve a lift-to-drag ratio commensurate with that of fully wetted hydrofoils ($L/D \simeq 15$).[8] The high cruise speed of 60 knots would be the normal mode of fast operation. At this speed, the foil would be fully ventilated. The burst speed capability at 80 knots would be of very limited duration, and would be achieved by operating the foils with a lower surface spoiler to reduce the lifting area.

The design is based on the analytical work of Furuya[9] describing an exact nonlinear numerical solution to the problem of two-dimensional gravity-free incompressible potential flow around an arbitrarily shaped supercavitating hydrofoil near a free surface. The high speed design conditions selected were a design lift coefficient of 0.20 at 60 knots for a fully ventilated flow. An aspect ratio of 5 was selected on the basis of experience, since that was the largest aspect ratio at which a supercavitating foil could be built with single strut support. The basic section was determined by varying the input parameters in Furuya's computer program. This program assumes that the forward lower surface profile is made up of a leading edge ellipse of radius R_c. The remainder of the lower surface profile is a circular arc, blending smoothly with the ellipse, as shown in Figure 1. The lower surface transition from negatively cambered ellipse to positively cambered arc occurs at a distance x_c from the leading edge. At x_c, the lower foil surface slope, with respect to the foil reference line, is zero. The upper surface separation point is at $x = x_B$. Unrelated to foil geometry is the parameter α_z, which is the angle between the foil reference axis and the direction of the far field flow. It is therefore an angle of attack. The angle ϕ is the angle subtended at the center of the circle. the lower surface was determined by a systematic variation of the geometrical parameters. The final design section was

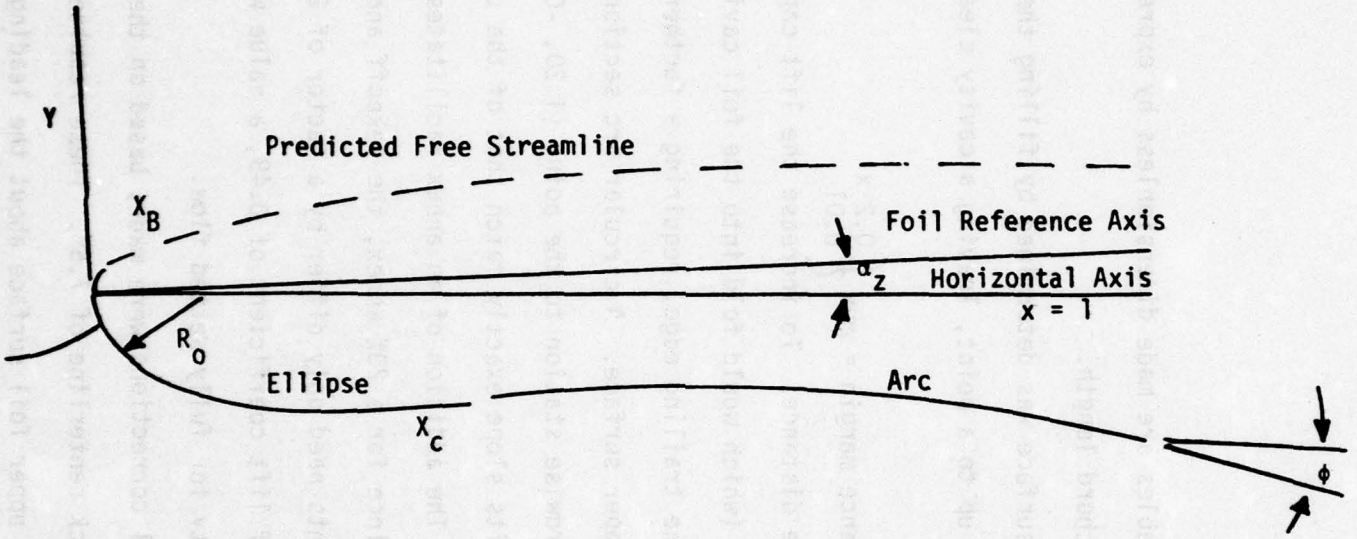

Figure 1 - Section Layout for Furuya's Computer Program

$R_o = 0.0009$

$x_B = 0.0009$

$x_c = 0.20$

$\phi = 12°$

$\alpha_z = -2.5°$,

where all length variables are made dimensionless by expressing them as a fraction of the chord length.

The basic upper surface was determined by filling the cavity above the camber line up to a point, leaving a cavity clearance margin chosen to be

$$\text{cavity clearance margin} = \max \begin{cases} 0.2\,x \\ 0.01 \end{cases}$$

where x is a chordwise distance. To increase the lift capability at takeoff, a large flap (which would fold into the foil cavity at high speed) is fitted at the trailing edge, requiring a further modification to the upper surface. A circular arc section was fitted from the x = 0.70 chordwise station to the point (1.20, -0.08) with the requirement that its slope exactly match that of the upper surface at x = 0.70. The addition of an annex facilitates the overall design task since for a 20% annex, the takeoff and cruise design lift coefficients need only differ by a factor of 2.45, resulting in a takeoff lift coefficient of 0.49, a value which is well within possibility for fully wetted flow.

Three-dimensional corrections were made, based on the aspect ratio of 5.0 and a sweepback centerline of 7.5°. These resulted in a spanwise twist of the upper foil surface about the leading edge line.

The strut used with the TAP-2 hydrofoil has already been experimentally evaluated.[11] In its basic configuration, it is a fully wetted NACA 16-012 section. For high speed operation, ventilation wedges extend from its sides and convert the strut into a blunt-based section. These wedges are attached just behind the widest part of the strut and extend to 70% of the strut chord. They provide a path for the passage of air to the foil. The strut sweepback angle is 8°. Figure 2a shows section shapes for the strut and foil. Tables of offsets are given in Appendix A. Figure 2b shows the entire TAP-2 system.

For the TAP-2 foil, 60 knots is the high speed design point where the foil should operate fully ventilated with no flap down. At the condition of burst speed of 80 knots, the problem is to reduce the dynamic lift which has increased as the square of the speed. This is solved by using a lower surface wedge, or flow spoiler, to separate the lower flow from the foil and thus reduce the lifting area. The final design arrived at calls for a spoiler of length 0.1 situated at the $x = 0.45$ chordwise station and an inclination angle of 12°. At 80 knots, the predicted two-dimensional design lift coefficient is 0.153 and the lift-to-drag ratio is 15.3.

EXPERIMENTAL

Two models of TAP-2 were built and tested. One was constructed with a takeoff annex and tested at low speeds by the David Taylor Naval Ship

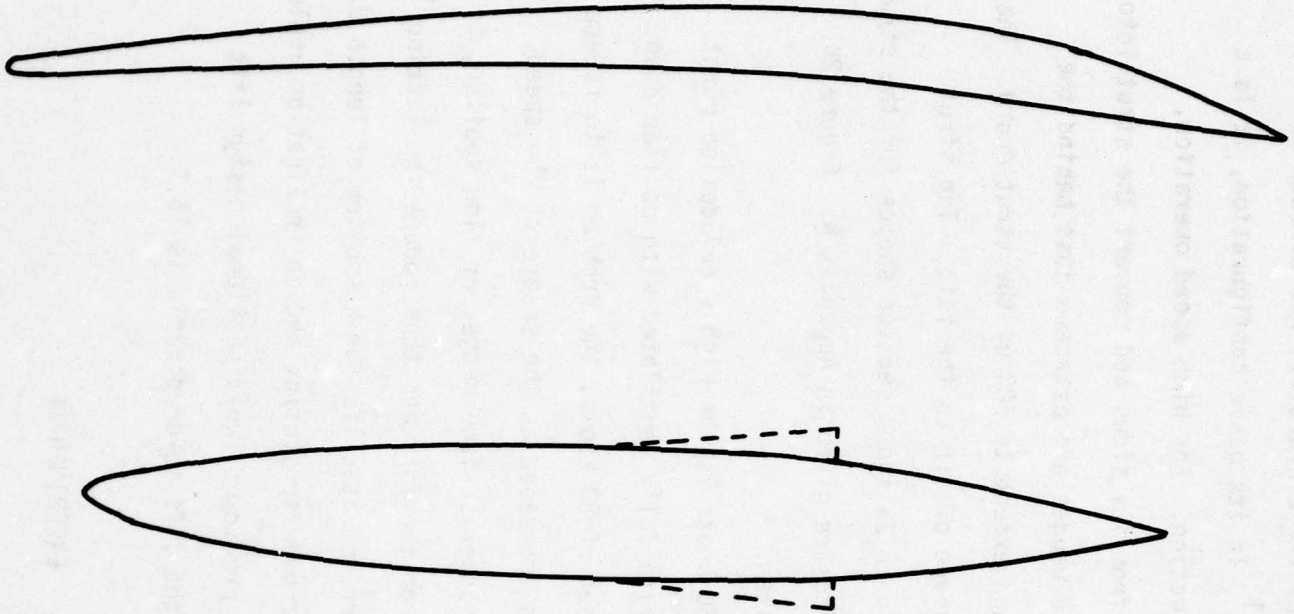

Figure 2a- Sketches of the Basic TAP-2 Hydrofoil Section, and of the Modified NACA 16-012 Strut Used with it. Strut is Shown with Ventilated Wedges

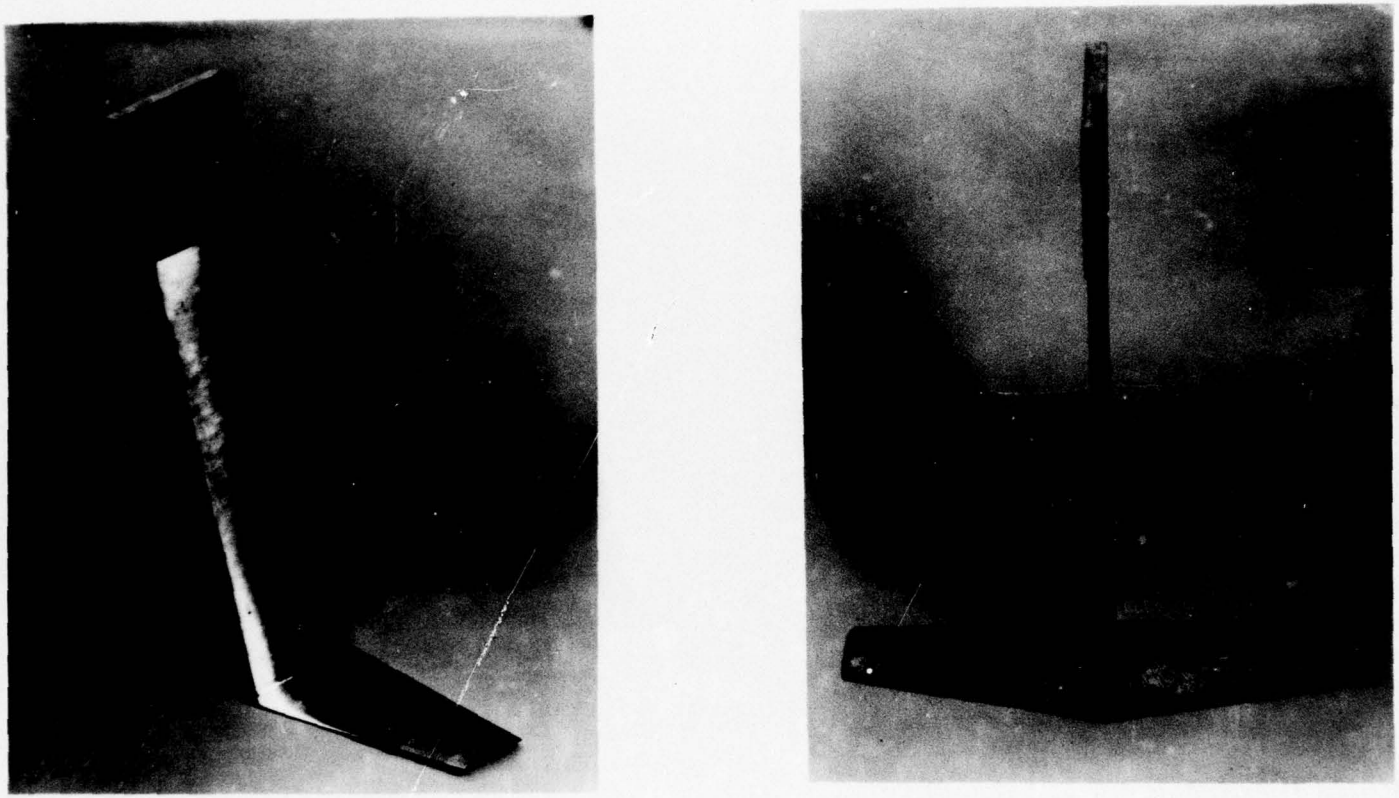

Figure 2b - TAP-2 Strut-Foil System

Research and Development Center (DTNSRDC) at Langley Field.[6] Another model, without annex but with strut spray wedges, was tested by Lockheed in their variable pressure towing tank, the Lockheed Underwater Missile Facility (LUMF).[7] This chapter describes the models, test facilities and experimental conditions.

THE DTNSRDC LOW SPEED TESTS

The TAP-2 foil model for this experiment was constructed with a trailing edge flap to provide additional lift capability during takeoff. The flap area was approximately equal to 20% of the total area. For all practical purposes, the entire foil-flap system can be considered as one foil with reduced aspect ratio. This is the view adopted here.

The tests were performed in Langley Tank No. 1 of DTNSRDC. A detailed description of the facility can be found in Reference 12. Foil geometrical characteristics as well as the range of experimental variables pertaining to this experiment are given in dimensionless form in Table 1. Table 2 gives the dimensional constants relevant to both tests.

The basic DTNSRDC data consist of a tabulation of lift, drag and pitch moment measured under the experimental conditions outlined in Table 1. These numbers are supplemented by photographs showing the extent of cavitation.

TABLE 1
RANGE OF EXPERIMENTAL PARAMETERS

Experimental Parameter	DTNSRDC (Reference 6)	LUMF (Reference 7)
STRUT-FOIL SYSTEM		
Total foil planform area, A	4.17	5.00
Foil tip chord	0.67	0.67
Foil root chord	1.33	1.33
Foil mean chord, c	1.00	1.00
Foil span, L	4.17	5.00
Foil aspect ratio, AR	4.17	5.00
Foil taper ratio	0.50	0.50
Strut chord	1.11	1.33
FLOW CONDITIONS		
Speed range (knots), V_o	30 to 50	11 to 22.5
Vapor cavitation number, σ_v	0.30 to 0.89	0.17 to 0.35
Depth-to-chord ratio, h/c	1 to 3	0.5 to 2
Chord Froude number, $N_{F,c}$	13 to 22	5 to 11
Depth Froude number, $N_{F,h}$	7.6 to 22	5 to 15
Angle of attack (degrees), α	-2 to 7	-2 to 8
Angle of yaw (degrees)	0	0 to 7.5

TABLE 2
DIMENSIONAL CONSTANTS APPROPRIATE FOR THE
DTNSRDC AND LUMF EXPERIMENTS

Constant	DTNSRDC (Reference 6)	LUMF (Reference 7)
Foil mean chord, c	0.450 ft 0.137 m	0.375 ft 0.114 m
Water density, ρ	1.97 sl/ft^3 1015 kg/m^3	1.97 sl/ft^3 * 1015 kg/m^3 *
Acceleration of gravity, g	32.17 ft/sec^2 * 9.81 m/sec^2 *	32.17 ft/sec^2 * 9.81 m/sec^2 *
Atmospheric pressure, p_{atm}	2116 lb/ft^2 * 101.3 kPa *	2116 lb/ft^2 * 101.3 kPa *
Water vapor pressure, p_v	22.1 lb/ft^2 * 1.058 kPa *	35.6 lb/ft^2 * 1.705 kPa *

* Denotes assumed values

THE LOCKHEED SCALED HIGH SPEED TEST

The LUMF consists of a towing carriage enclosed in a variable pressure atmosphere. Low cavitation number may be achieved by reducing the ambient pressure. The LUMF data[7] include dimensionless force coefficients (lift, drag, pitching moment and strut side force) and pressure coefficients measured at locations where a cavity should form: at the strut base and on the foil near the strut-foil intersection. No dimensional data are given.

The LUMF makes possible simultaneous scaling of Froude and cavitation numbers. The LUMF data are given as functions of a scaling parameter relating the test measurement to a hypothetical foil whose size and speed are related to the model size through this scaling factor. Since the physical dimensions (other than the flap) for the DTNSRDC and LUMF foil models were identical, the LUMF scaling parameter is not extensively used in the present data analysis. Rather, we choose to view the LUMF experimental results as pertaining to a single strut-foil system under a variety of cavitation and Froude numbers.

The tests were conducted with deployed ventilation wedges.

The nondimensional coefficients used in this report are consistent with the original data reports[6,7] and are defined in the Nomenclature.

Difficulties experienced with pressure measurements unfortunately preclude the use of cavity cavitation number as a correlating parameter. Four pressure transducers were symmetrically placed, two on the upper foil surface and two at the base of the strut. The LUMF

final report[7] states that "the reliability of the pressure measurements was apparently rather variable." No cause for the lack of reliability is given. For any given flow conditions, the pressure coefficients reported by symmetrically placed transducers should be roughly equal. Yet, such measurements were found to differ by factors of two, even up to ten or greater. Without the cavity cavitation number, a choice correlation parameter for ventilated flow, the analysis was done using the vapor cavitation number.

The reader's attention must be called to the important fact that TAP-2 is a variable geometry system, and the interpretation of experimental results must be made with this in mind. The DTNSRDC model, built with a trailing edge flap, accurately represents TAP-2 at takeoff. The same model, tested at low speed cruise speeds may result in excessive lift since the flap is not normally used at these speeds. Similarly, the LUMF model gives results that are applicable to TAP-2 only when actually ventilated. Some data are given for models tested in unrepresentative flow conditions. Since this work is of an exploratory nature, such data are presented, but their actual applicability to an operational strut foil system is limited.

TAKEOFF PERFORMANCE

In his experimental report[6] on TAP-2 takeoff, Holling states that cavitation was observed on the foil. The photographs included with his report clearly show incipient leading and trailing edge cavitation.

Depth effects were found to be small by Holling. We find it possible to collapse the experimental data for various depth-to-chord ratios (h/c = 1,2,3) onto universal curves by including depth effects as affecting the hydrostatic pressure in the cavitation number. In other words, the effect of depth is to change σ_v. Figures 3-5 show an excerpt of the data reduced in this fashion. Figure 3 shows the variation of C_L versus σ_v for various choices of angle of attack. Other angle of attack runs are not included because of crowding. At high values of the vapor cavitation number, C_L remains constant for the flow is fully wetted: the lift increases with the square of the foil speed. As the cavitation number is decreased, cavitation manifests itself on the foil and C_L decreases. The arrow in Figure 3 indicates the takeoff condition, and coincides with the onset of cavitation, as evidenced by a tendency for lower values of C_L as σ_v decreases. This correlates well with reported visual observations.[6] The solid lines in Figures 3 to 5 are meant to guide the eye, and were not determined by any mathematical rule.

TAP-2, designed to take off in the fully wetted mode, actually experiences limited cavitation. As the speed increases, the effect of cavitation on lift becomes more pronounced.

TAP-2 was designed to have a lift coefficient of 0.2 at 60 knots (without flap). To support the same load at 35 knots (with flap) requires, according to Baker,[5] a takeoff lift coefficient of 0.49. As speed is increased, lesser lift coefficient is required. The

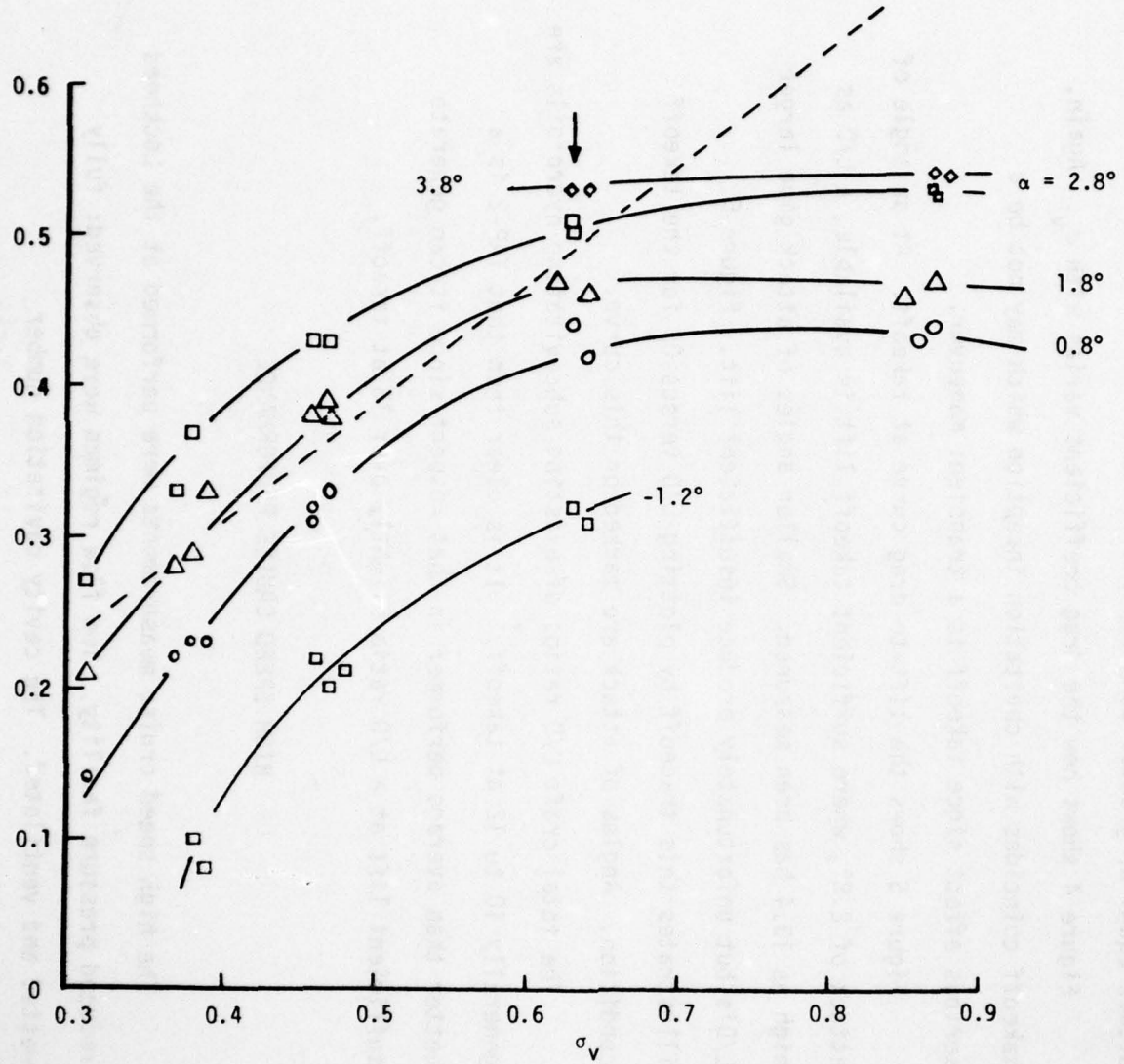

Figure 3 - Takeoff Lift Coefficient, TAP-2

dotted line on Figure 3 represents the lift coefficient (with flap) required to support the design load. Clearly, more than enough lift is generated to satisfy takeoff requirements, at least for angles of attack equal or greater than 2.5°.

Figure 4 shows how the drag coefficient varies with σ_v. Again, takeoff coincides with cavitation inception which may not be a serious effect since takeoff is a transient maneuver.

Figure 5 shows the lift-to-drag curve at takeoff. At an angle of attack of 2.8°, where sufficient takeoff lift is available, a L/D as high as 13.4 has been measured. Smaller angles of attack give larger L/D's but unfortunately produce insufficient lift. Figure 6 illustrates this tradeoff by plotting L/D versus C_L for the takeoff condition. Angles of attack are marked on this curve.

The total craft L/D ratios of existing subcavitating hydrofoils are generally 10 to 12 at takeoff.[1] It is clear then that TAP-2 is a better than average performer in that respect since it can generate sufficient lift at a L/D ratio slightly over 13 at takeoff.

HIGH SPEED CRUISE PERFORMANCE

The high speed cruise measurements were performed at the Lockheed reduced pressure facility. Two flow régimes were observed: fully wetted and ventilated. The cavity cavitation number

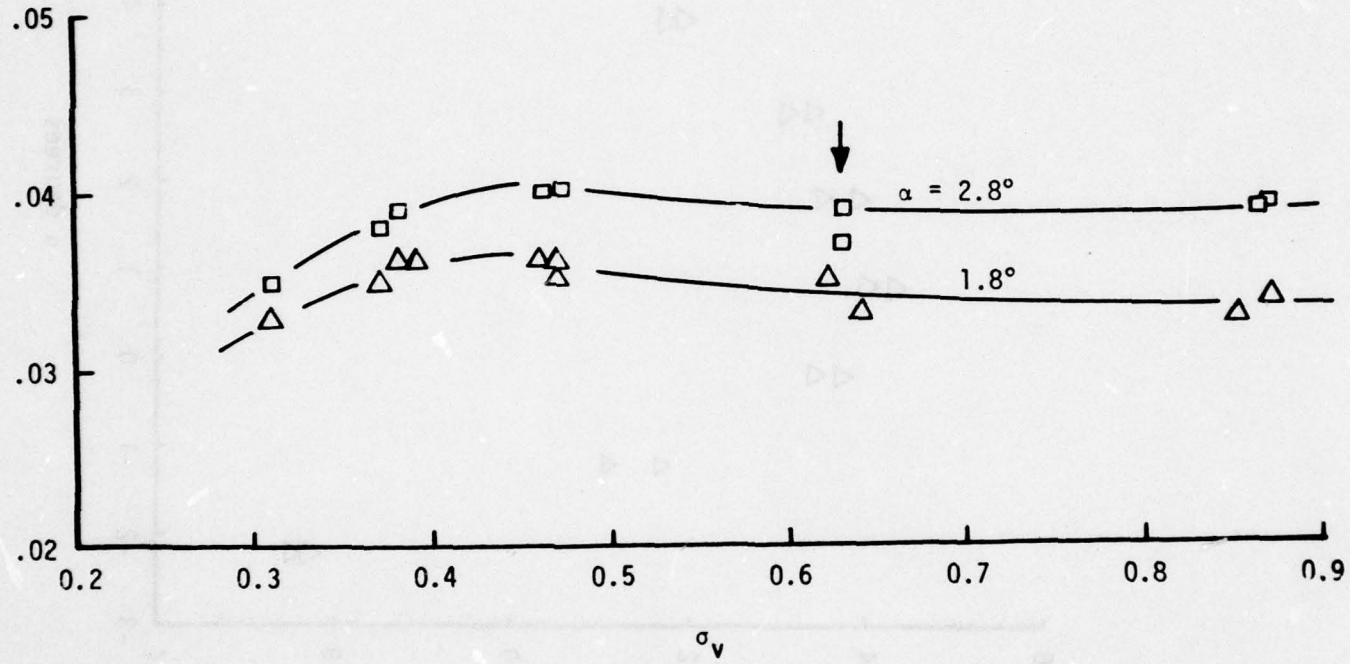

Figure 4 - Takeoff Drag Coefficient, TAP-2

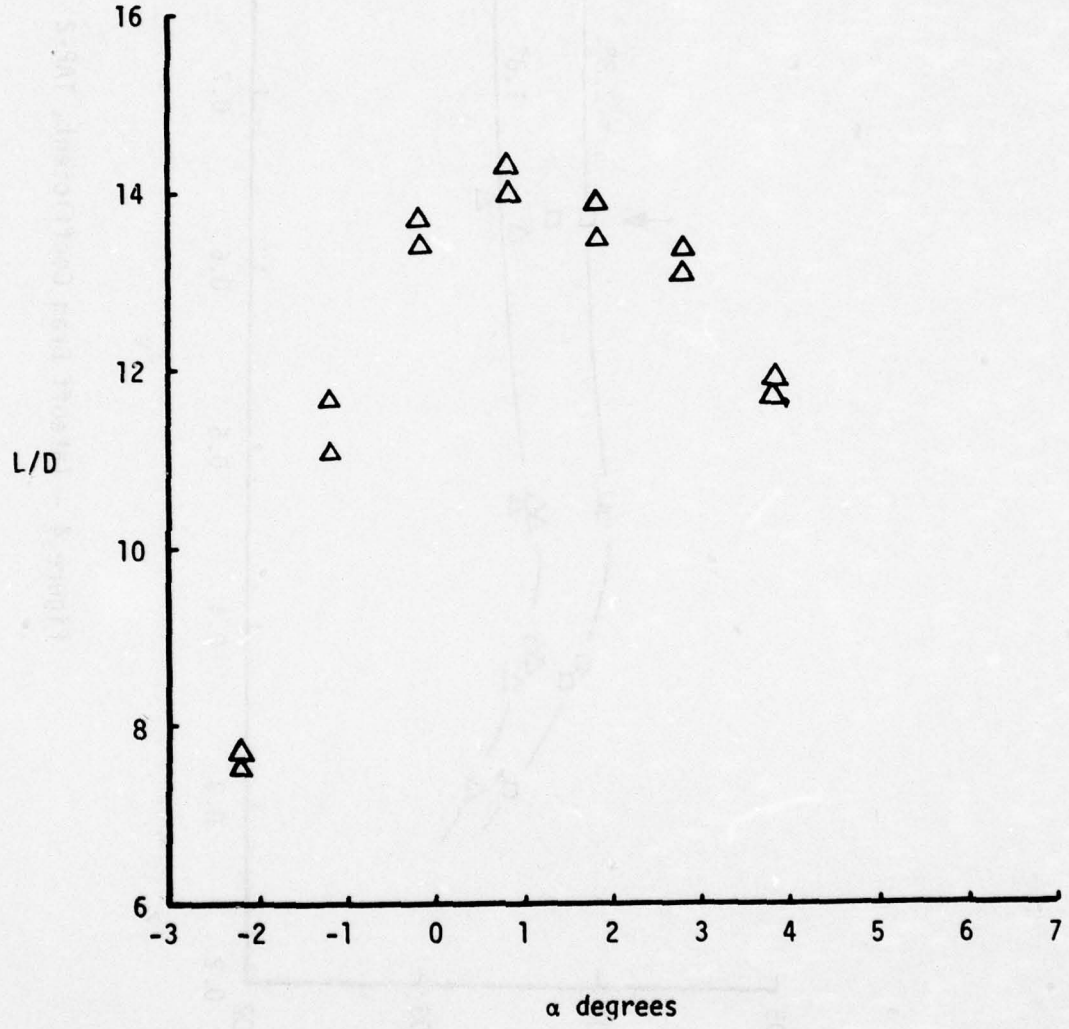

Figure 5 - TAP-2 Takeoff Lift-to-Drag Ratio, σ_v = 0.62

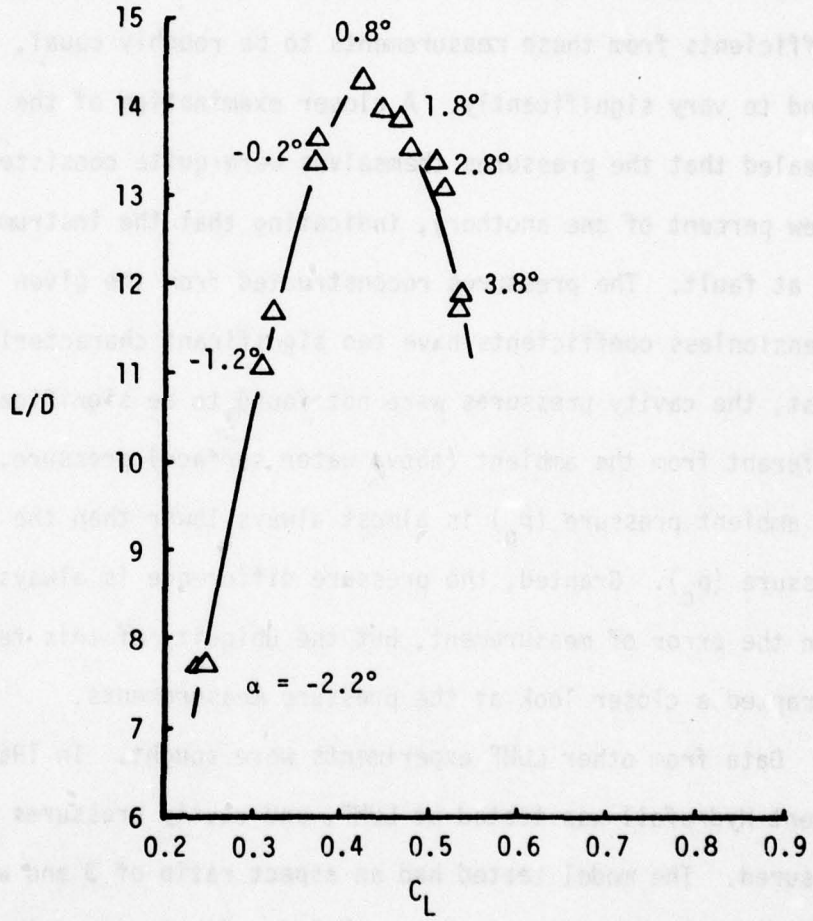

Figure 6 - TAP-2 Takeoff Lift-to-Drag Ratio, σ_v = 0.62

$$\sigma_c = \frac{p_o + \rho g h - p_c}{\frac{1}{2}\rho V_o^2}$$

would then be the choice correlation parameter. Unfortunately, the cavity pressure measurements cannot be used for that purpose. Four pressure transducers were placed symmetrically on the model: two on the upper foil surface and two at the strut-foil intersection near the strut base. Whereas one might expect the four pressure coefficients from these measurements to be roughly equal, they were found to vary significantly. A closer examination of the data revealed that the pressures themselves were quite consistent (within a few percent of one another), indicating that the instrumentation is not at fault. The pressures reconstructed from the given dimensionless coefficients have two significant characteristics. First, the cavity pressures were not found to be significantly different from the ambient (above water surface) pressure. Second, the ambient pressure (p_o) is almost always lower than the cavity pressure (p_c). Granted, the pressure difference is always smaller than the error of measurement, but the ubiquity of this feature warranted a closer look at the pressure measurements.

Data from other LUMF experiments were sought. In 1965, the BUSHIPS Parent Hydrofoil was tested at LUMF, and cavity pressures were measured. The model tested had an aspect ratio of 3 and was approximately of the same size as TAP-2. Exact geometrical correspondence is not required here, as we seek only general trends in the pressure measurements. Two parameters are used here. First,

we form a dimensionless pressure difference parameter

$$\xi = \frac{p_o - p_c}{\rho g h}$$

where p_o is the air pressure above the water surface, p_c is the cavity pressure, and h is the depth of submergence. At LUMF, p_o may be equal to or less than p_{atm}, the atmospheric pressure. Second we use a scale parameter proposed by Kramer[7]

$$\lambda = \frac{p_{atm} - p_v}{p_o - p_v}$$

in the TAP-2 report. When Froude and vapor cavitation number scaling are simultaneously achieved, λ is equivalent to a model scale ratio. However, scaling is not of immediate interest here. We can view λ as an ambient pressure parameter. Figure 7 shows $\xi(\lambda)$ for the LUMF test of the BUSHIPS Parent Hydrofoil. The data are plotted indiscriminately and represent various angles of attack and Froude numbers. The angle of attack is not reported here since the details of the actual model is of no concern to this discussion. Next to each data point is a number indicating the depth Froude number for that measurement. From these observations, we learn that there is an upper limit to the cavity-ambient pressure difference. This limit is large (tens of hydrostatic pressure heads) at atmospheric pressures but rapidly decreases as the ambient pressure is decreased. The TAP-2 tests were performed at λ = 10, 15 and 20 (arrows on Figure 7). At such reduced pressures, the pressure difference is smaller than the experimental error and may therefore be considered zero. The

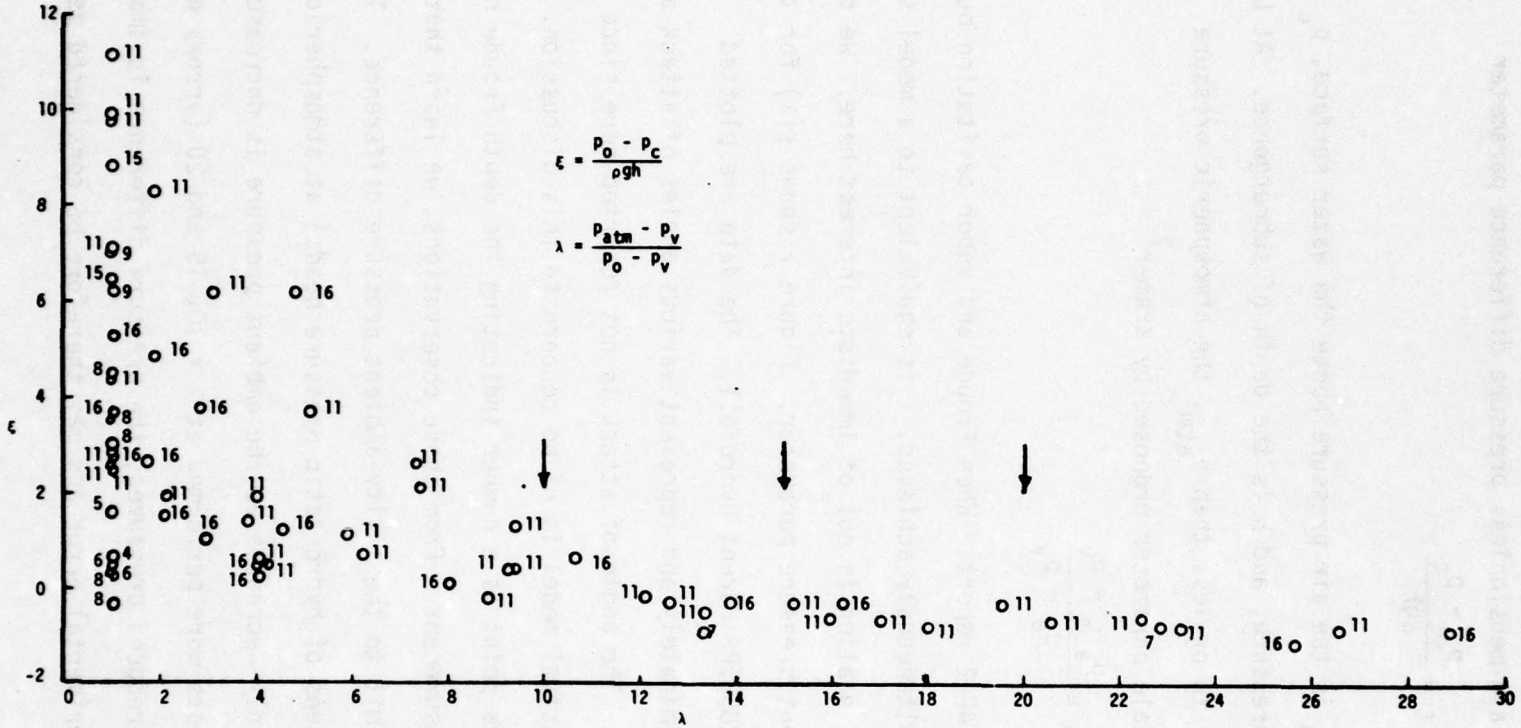

Figure 7 - Cavity Pressure Correlation for the BUSHIPS Parent Hydrofoil Tested at the LUMF. (The Depth Froude Number is Indicated Next to Each Point.

negative pressure differences observed for $\lambda > 12$ seem to indicate that cavity pressures exceed ambient pressures. The effect is, as noted, smaller than can be accurately resolved, and could be attributed, for example, to a small error in measuring the ambient pressure.

There appears to be no consistent distribution of data points according to Froude number on that figure. We take this to mean that once the flow was established after the carriage was set in motion, the particular degree of ventilation was little influenced by gravity.

We can therefore surmise what conditions may have prevailed during the TAP-2 test. At the chosen ambient pressures, the cavity pressure cannot be expected to significantly differ from the ambient pressure. Therefore, this leaves

$$\sigma_c = \frac{p_o - p_c + \rho gh}{\frac{1}{2}\rho V_o^2} = \frac{\rho gh}{\frac{1}{2}\rho V_o^2} = \frac{2}{N_{F,h}^2}$$

since $p_o \simeq p_c$. The magnitude of the hydrostatic pressure head however is itself smaller than the pressure measurement errors so that no reliable value for σ_c can be deduced from measurements. This is clearly reflected in the lack of consistency between the four values of C_p reported for each run.

The phenomenon of ventilation, on which TAP-2 relies, is not fully understood and depends on a large variety of parameters, not all of which are measured in any given test facility. The accepted parameter on which correlations are based is the cavity cavitation

number. There are other parameters, however, such as the ventilation index[16,17]

$$K_v = \frac{Q_{air}}{AV_o}$$

where Q_{air} is the volumetric air flow rate entrained into the cavity, A is the vertical projection of the foil area, and V_o is the foil speed; the depth Froude number

$$N_{F,h} = \frac{V_o}{\sqrt{gh}}$$

where h is the depth of submergence; and the Reynolds number

$$N_R = \frac{cV_o}{\nu}$$

where ν is the liquid kinematic viscosity. Some measure of the air content should also be considered.

Faced with the impossibility of describing the experimental results in terms of scaling parameters which would allow extrapolation to dynamically similar conditions, we must accept the admittedly less than ideal situation of describing as completely as possible the conditions prevailing at the time of the test. We shall therefore adopt σ_v, the vapor cavitation number, as a parameter. It actually represents a speed (or pressure) coefficient indicating the ratio of the ambient static to dynamic pressure, and does not provide any information about the average pressure inside the cavity. Using σ_v as a parameter, a direct indication of the behavior of the foil over a speed range is obtained.[18] We must make an important distinction between a "scaling parameter," which correlates model data to

dynamically similar full scale conditions, and a "parameter," which does not. We use σ_v as a simple parameter and at no time do we apply performance results to conditions other than those present at the time of the experiment. Without σ_c (and possibly other parameters) to define the ventilated condition, we cannot apply the LUMF results to other dynamically similar conditions simply because we lack the necessary information to define these conditions. As used in this analysis, σ_v must be understood to be a simple parameter, devoid of any correlating attributes. That is to say, replicating the same σ_v on a TAP-2 geosim in a towing basin, for instance, does not guarrantee the duplication of ventilation conditions or forces observed at LUMF.

The force (performance) measurements themselves are real enough and it would not be reasonable to disregard them for lack of a universal set of dynamic correlation parameters. The foil performance itself resides in the dimensionless force coefficients. It is the dynamic conditions under which such performance was obtained that are not precisely known.

The only data which, strictly speaking, pertain to TAP-2 at cruise speed, are those which were measured under fully ventilated conditions.

Throughout this analysis the vapor cavitation number is used as a parameter. The vapor cavitation numbers are clustered into six groups with nominal (mean) values of 0.13, 0.17, 0.22, 0.24, 0.32 and 0.34. For each group, the standard deviation of these σ_v's about their nominal values was 0.01 or smaller.

Figure 8 shows the unimportance of depth effects. Three sets of conditions, each held at constant α and σ_v but varying h/c are presented. Each case is represented by lift and drag coefficients, which were fit with linear least squares. The lift coefficient remains unchanged with depth of submergence, and the slight increase in C_D noted in two of the three data sets can be attributed to changes in the strut wetted area.

Figure 9 presents an overall look at the data. The foil is known to ventilate for $\alpha \geq 4°$. The variation of C_L with σ_v for $\alpha = -2°$, $0°$ and $1°$ are typical of cavitation incipience. Whether there actually was cavitation remains undetermined.

LIFT COEFFICIENT

Figure 10 shows the variation of the lift coefficient with angle of attack for various vapor cavitation numbers. The solid lines are piecewise linear least squares fit described by

$$C_L = \begin{cases} 0.134 + 0.139\,\sigma_v + 0.0606\,\alpha & -2° \leq \alpha \leq 1° \\ 0.139 + 0.132\,\sigma_v + 0.0164\,\alpha & 4° \leq \alpha \leq 8° \end{cases}$$

The change of slope, $\partial C_L/\partial\alpha$, at approximately $\alpha = 2°$ corresponds to a change in flow regime which is observed at that angle of attack: the flow changes from fully wetted to ventilated. The exact location of the cavity separation on the foil is not well defined. The angle of attack at which the flow ventilates is not clearly defined either, being somewhere between one and four degrees. This region is characterized by a scatter in C_L and a scarcity of data points. The

α	σ_v	C_L	C_D	
6	0.17	○	●	————
6	0.32	△	▲	– – – –
4	0.17	□	■	- - - - -

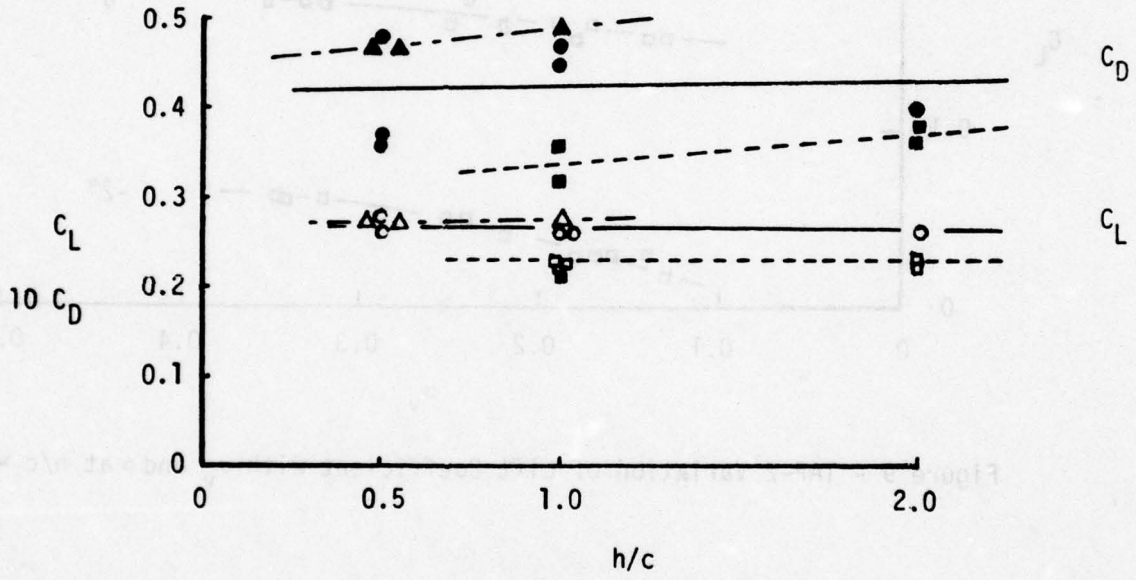

Figure 8 - TAP-2 Depth Effect, LUMF

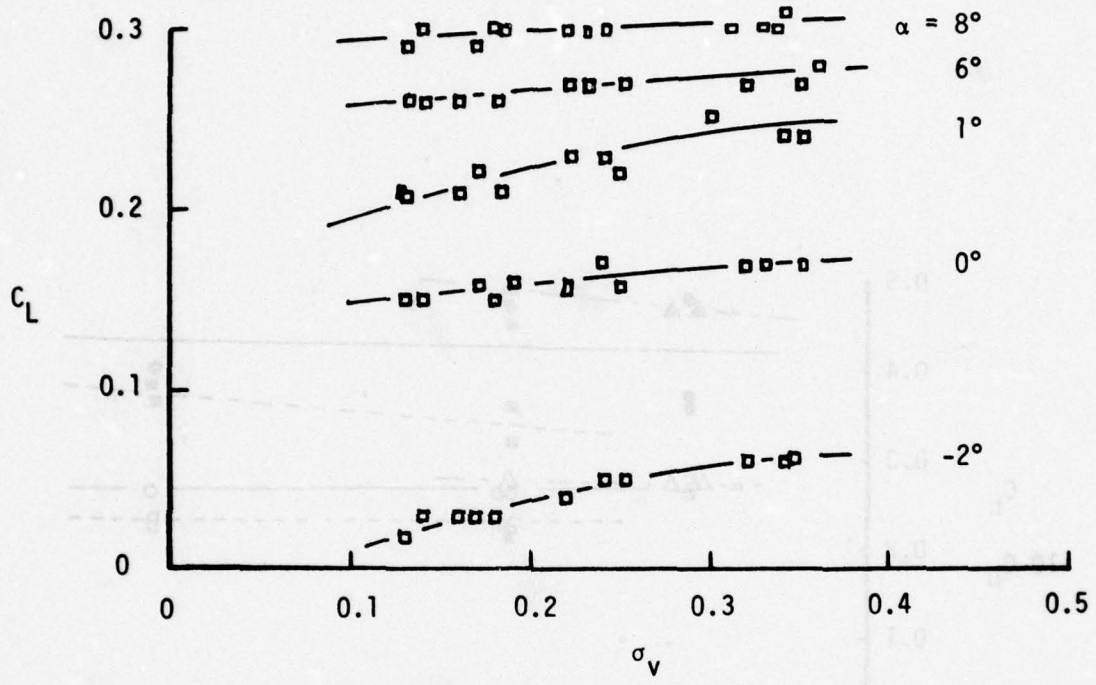

Figure 9 - TAP-2 Variation of Lift Coefficient with σ_v and α at h/c = 1

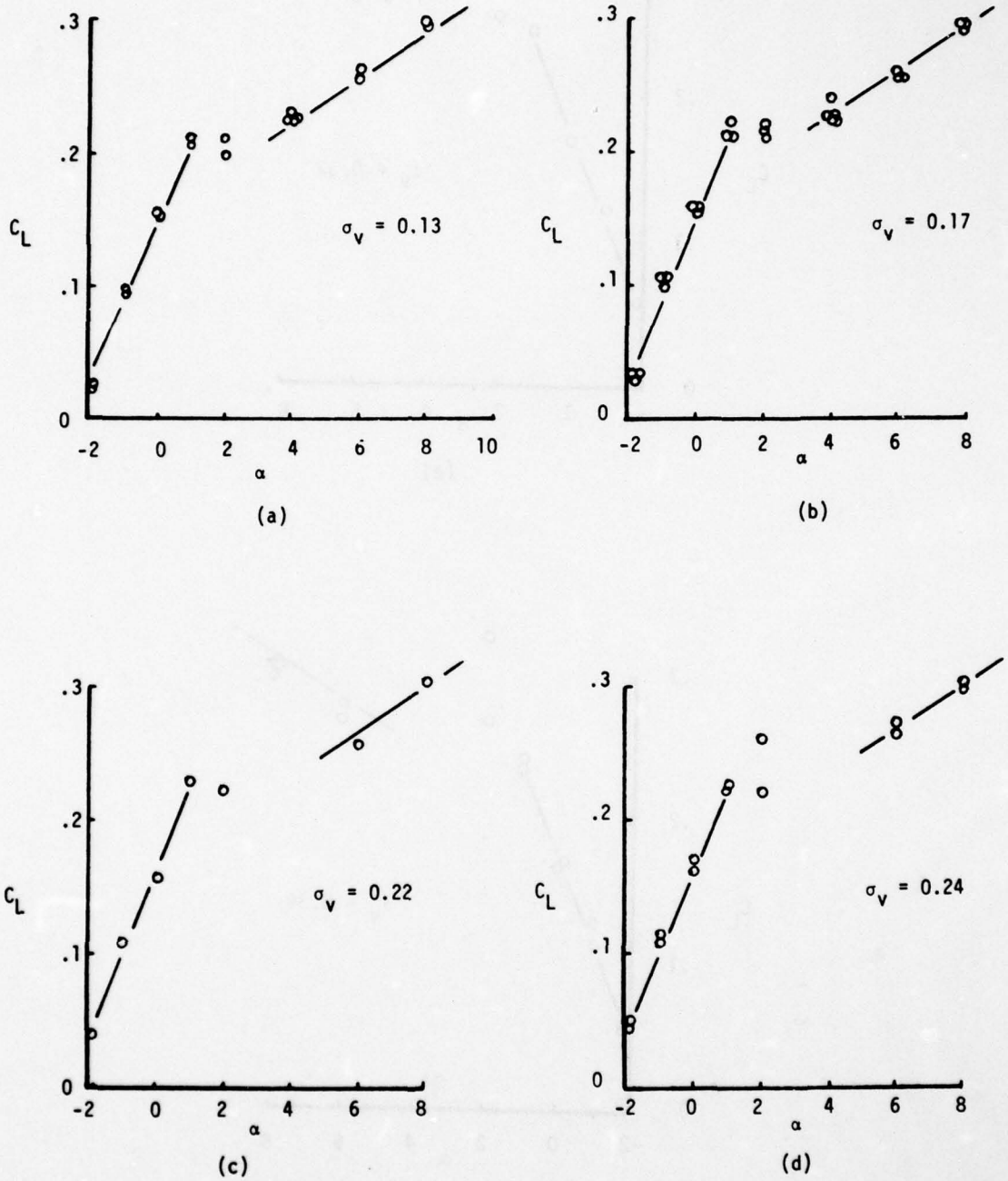

Figure 10 - TAP-2 Cruise Lift Coefficient, h/c = 1

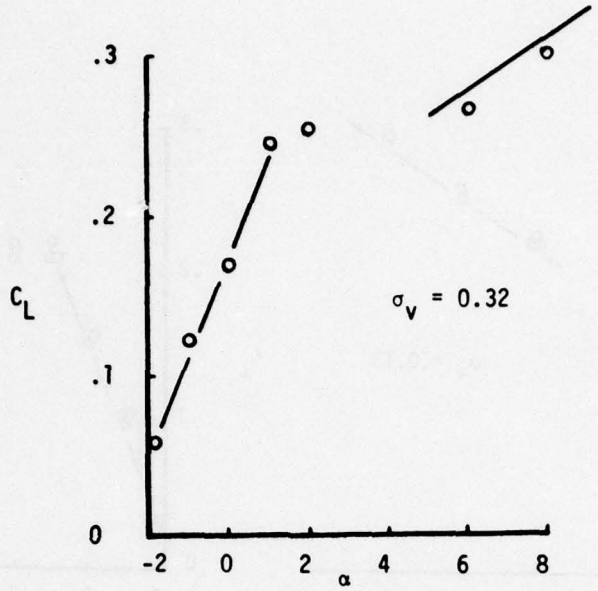

(e)

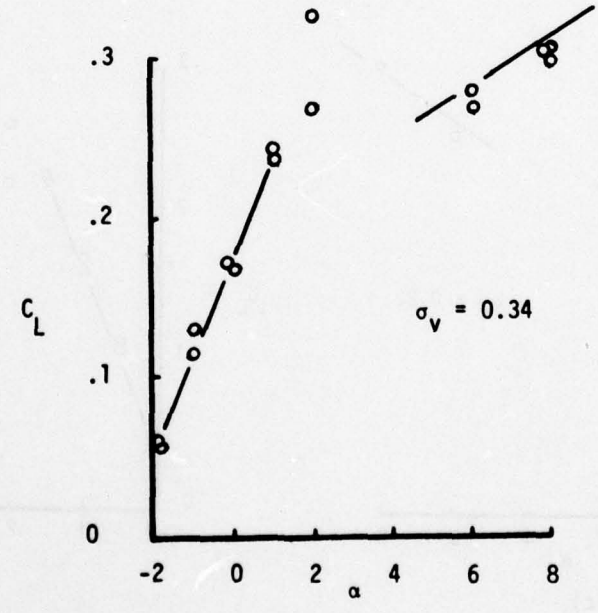

(f)

Figure 10 - (Continued)

reason for the "fuzziness" of the flow separation conditions has been attributed to a design error[14] whereby a flat cut is missing from the foil leading edge. The foil surface slope discontinuity at the prescribed cut would presumably have provided a site from which the cavity would spring. The nose shape of TAP-2 as it exists is a perfectly smooth and polished ellipse, that is, an airfoil nose.

The flow régimes of which we are certain are:

fully wetted for $\alpha \leq 1°$, ventilated for $\alpha \geq 4°$.

The dearth of measurements near the flow transition point is unfortunate since this is precisely where the largest ventilated lift-to-drag ratios are expected.

DRAG COEFFICIENT

Figure 11 shows the measured drag coefficients plotted as a function of angle of attack for the six values of σ_v considered. The solid lines are parabolas which were determined by least squares.

LIFT-TO-DRAG RATIO

The L/D ratio is plotted against angle of attack in Figure 12 and against lift coefficient in Figure 13. The solid lines are obtained from least squares fits of the lift and drag measurements. Restricting our attention to the fully wetted régime, we see that a L/D ratio of 8 to 12 is typical for TAP-2. A precise determination of the design point L/D ratio is unfortunately made difficult by the scarcity of data. However, for the two lowest vapor cavitation

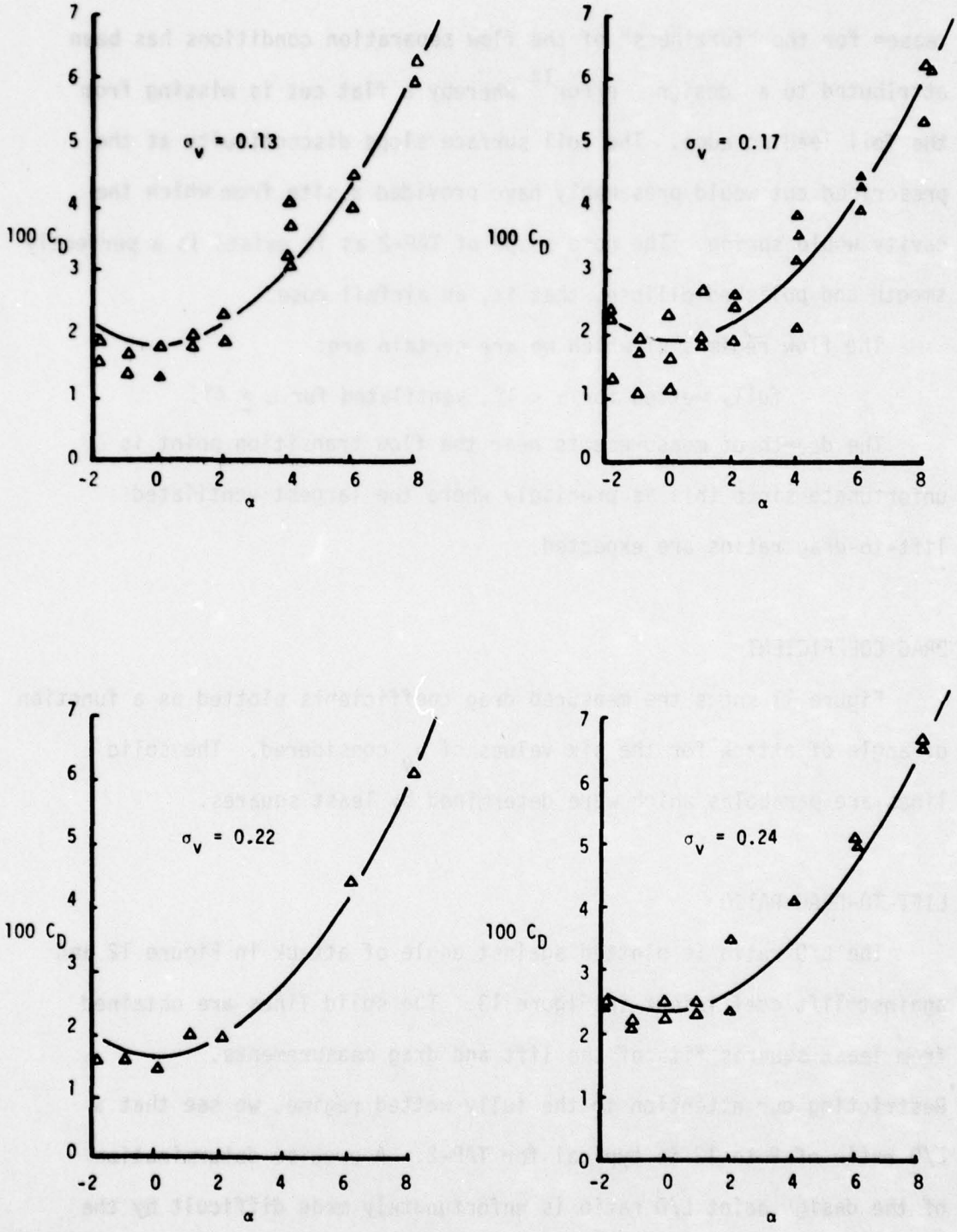

Figure 11 - TAP-2 Cruise Drag Coefficient, h/c = 1

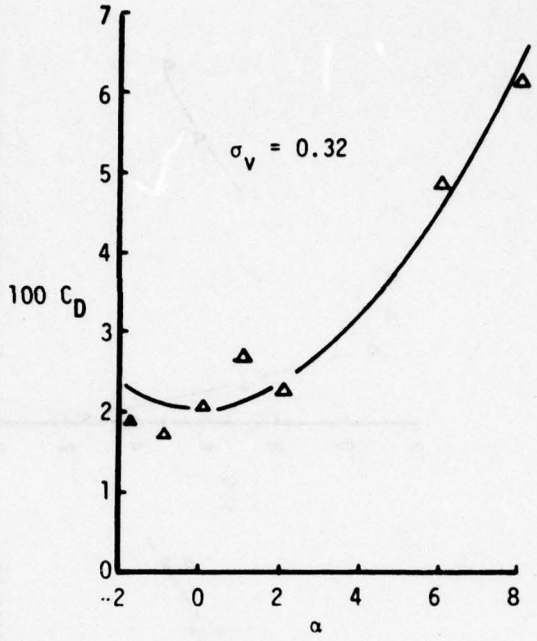

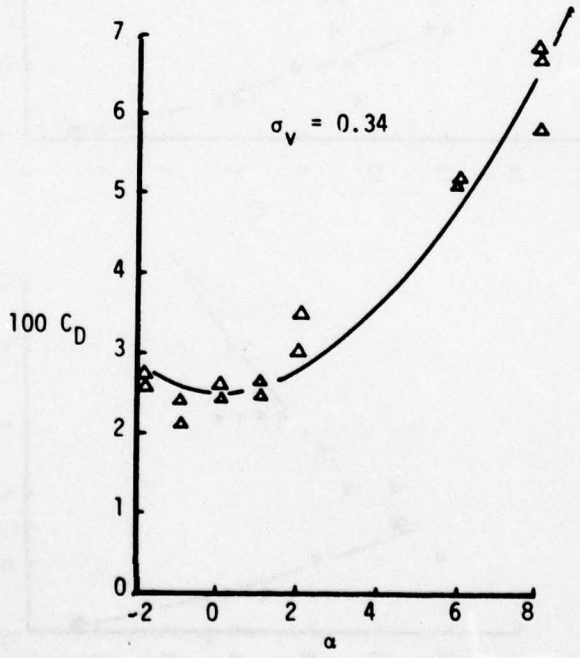

Figure 11 - (Continued)

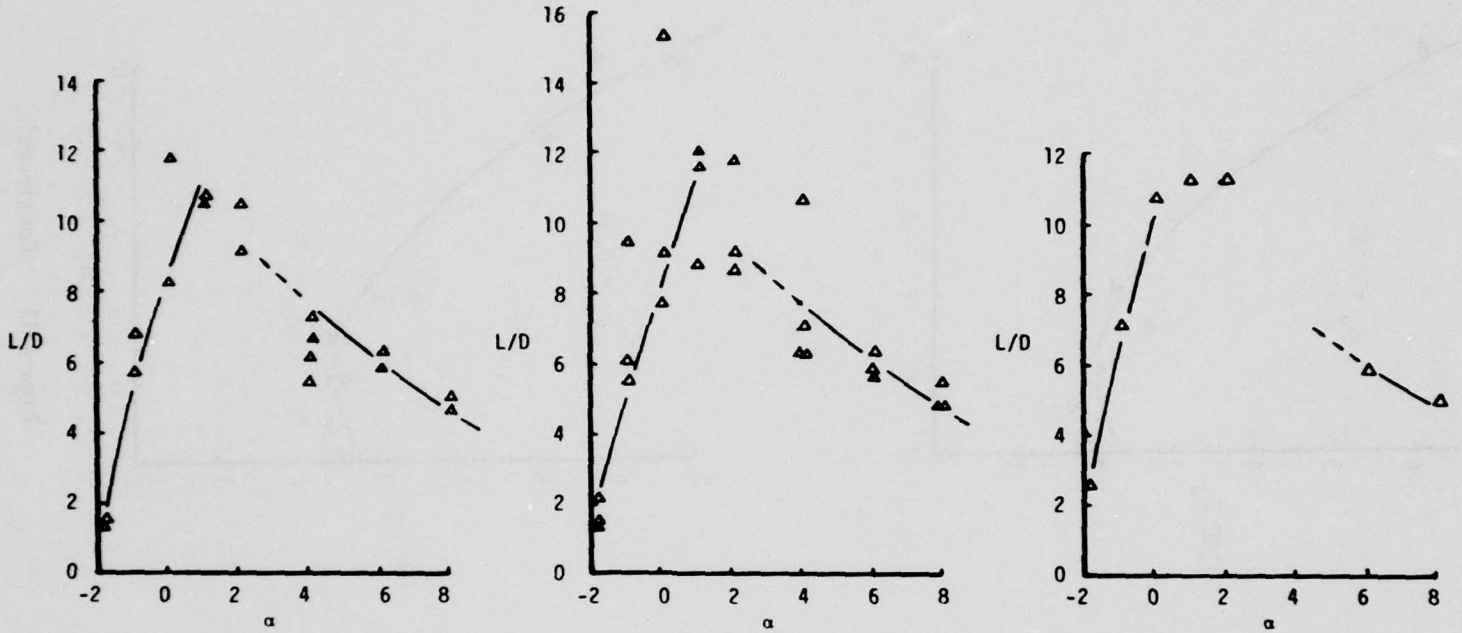

Figure 12 - TAP-2 Cruise, L/D Ratio

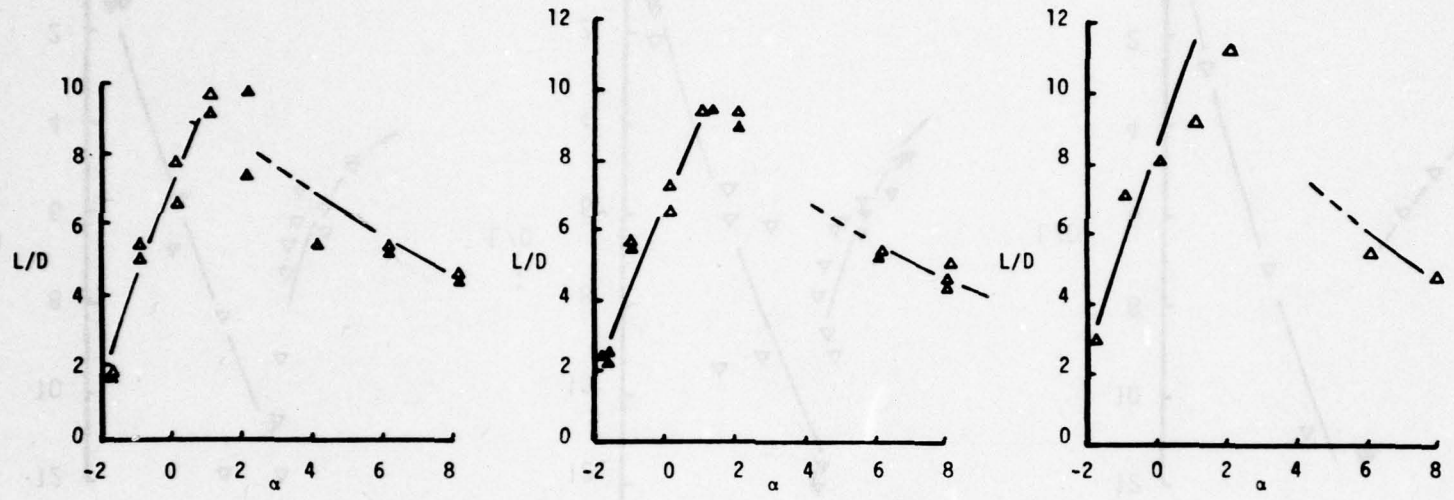

(a) $\sigma_v = 0.24$ (b) $\sigma_v = 0.34$ (c) $\sigma_v = 0.32$

Figure 12- (Continued)

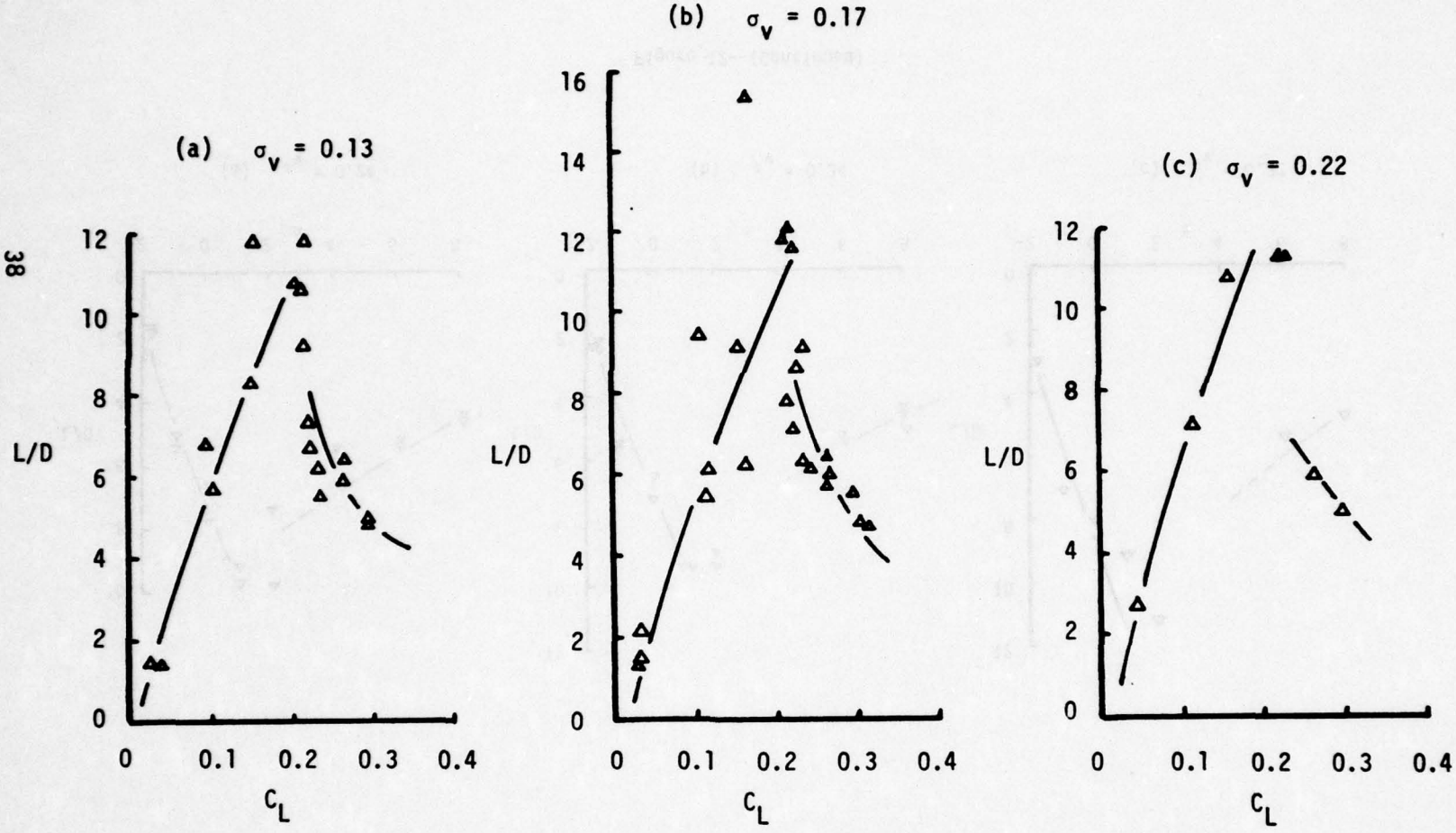

Figure 13 - L/D Ratios at Cruise

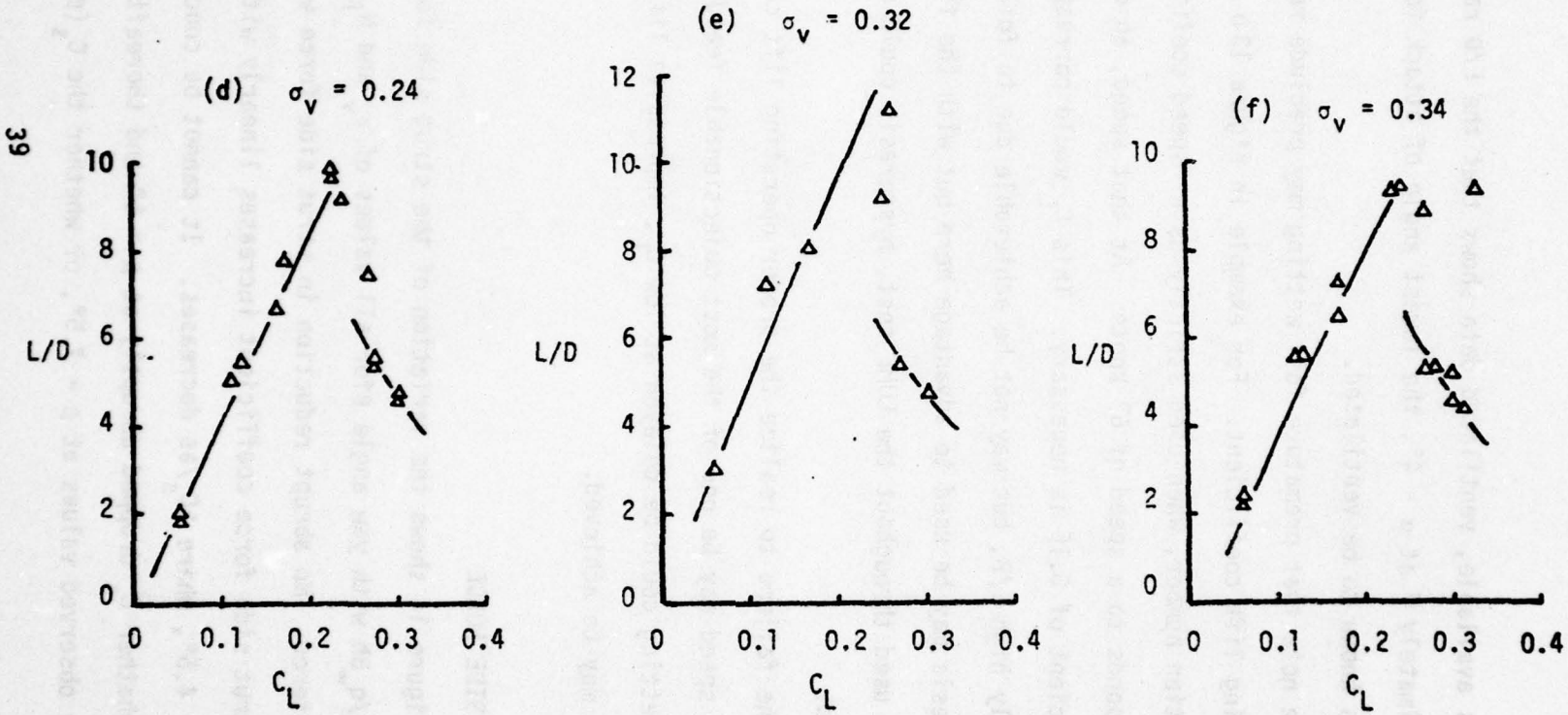

Figure 13 - (Continued)

numbers available, ventilated data shows that the L/D ratio is approximately 7 at $\alpha = 4°$, the lowest angle of attack for which the foil is known to be ventilated.

We note that premature foil wetting may preclude reaching the proper operating lift coefficient. For example in Figure 13b, vapor cavitation number, when used strictly as a "speed coefficient," corresponds to a speed of 67 knots. At that speed, an operating lift coefficient of 0.16 is necessary. This C_L would correspond to an enviably high L/D, but may not be achievable due to foil wetting. Hysteresis may be used to advantage here but with the fixed angles of attack used throughout the LUMF test, hysteresis could not be studied.

The failure to realize the proper operating lift coefficient at cruise speed may be one of the most objectionable features of TAP-2. If rewetting could be delayed at low C_L, impressive lift-to-drag ratios may be achieved.

STRUT SIDE FORCE

Figure 14 shows the variation of the strut side force coefficient $C_s = S/q_\infty Bh$ with yaw angle β for all values of σ_v and $N_{F,h}$ encountered. No abrupt reduction in strut side force was observed. The strut side force coefficient increases linearly with yaw angle up to $\beta = 4.5°$, where $\partial C_s/\partial\beta$ decreases. It cannot be concluded from the data whether C_s dropped abruptly at $\beta \sim 5°$ and thereafter increases to the observed values at $\beta = 7.5°$, or whether the $C_s(\beta)$ curve simply

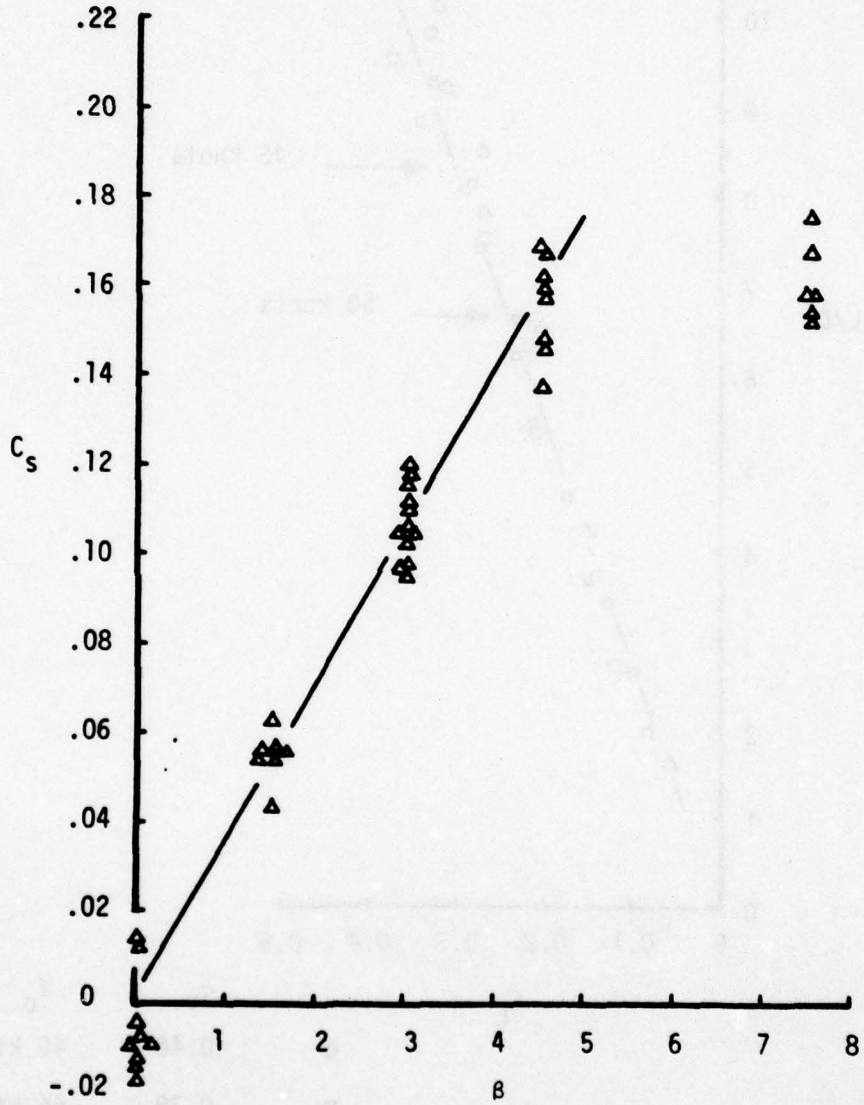

Figure 14a - TAP-2 Strut Side Force at h/c = 1

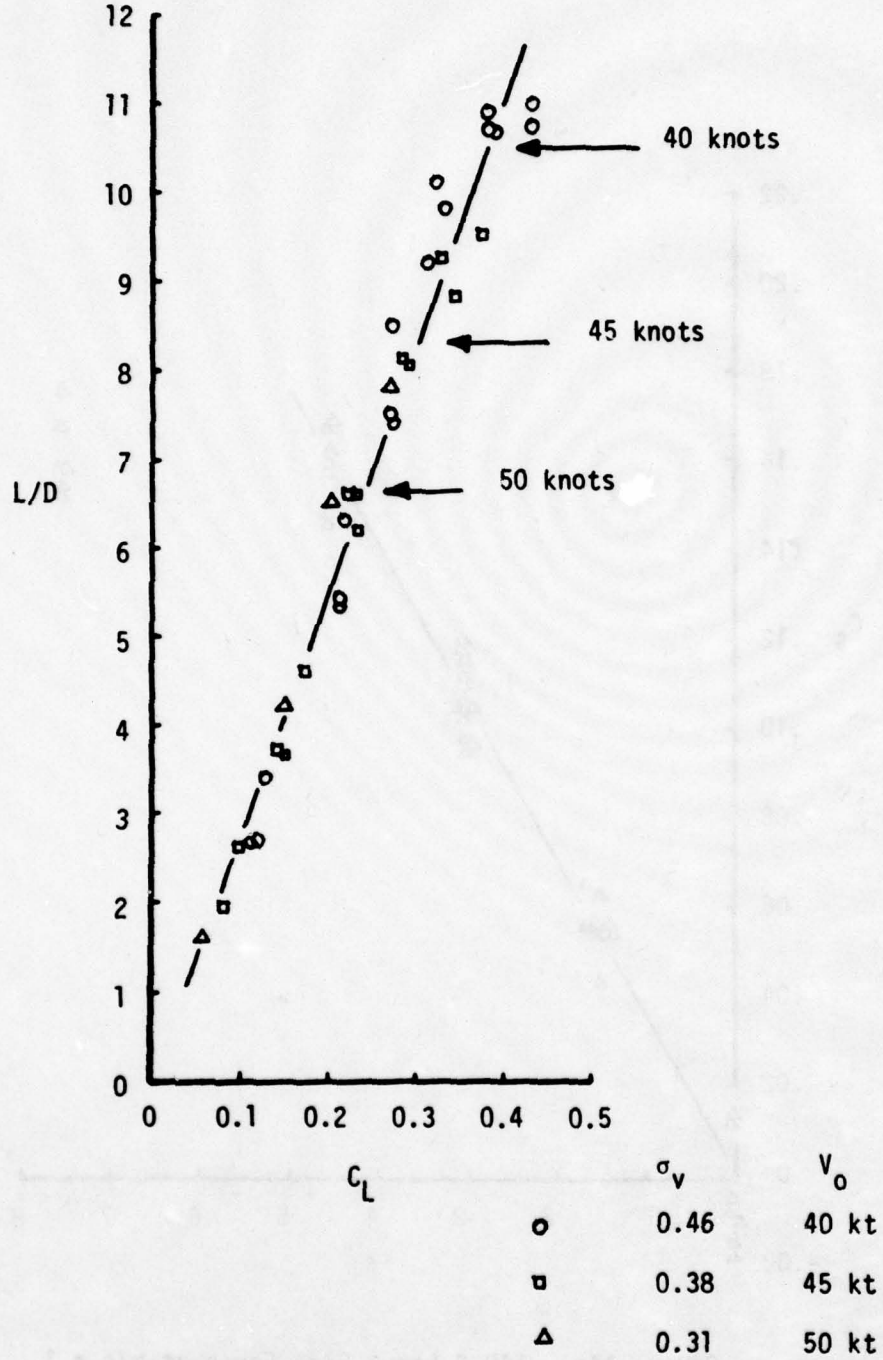

Figure 14b - TAP-2 Low Speed Cruise Performance

tapers off at $\beta = 5°$. This strut was previously studied by Nelka,[11] who noted that at high speeds, the slope $\partial C_s/\partial\beta$ tended to decrease from its constant value to zero until ventilation occurred.

LOW SPEED CRUISE PERFORMANCE

The low speed cruise range corresponds to vapor cavitation numbers from 0.3 to 0.5, taking into account speed and submergence variations, for an assumed cruise speed of 45 knots. The TAP-2 foil was designed to take off in the fully wetted flow mode with full flap extension, and to fly in the low speed cruise range with the flap partially retracted. At the high speed cruise (60 knots), the flap retracts completely into the super cavity existing in this range only.

The DTNSRDC model was built with the flap fixed in the fully extended position, in order to measure the takeoff performance; while the LUMF model was built without a flap, in order to simulate the high speed cruise condition. Therefore, the performance of the TAP-2 hydrofoil in the low speed cruise condition cannot be inferred directly from the LUMF and NSRDC experimental results.

Rather, when the NSRDC model (with full flap) is tested in this speed range, it is operating off-design by producing too much lift, and consequently suffers much cavitation and produces substantially more drag than it should. On the other hand, the LUMF model (with no

flap) when operated in this speed range, produces too little lift. Also, its configuration is such that the zero flap condition results in a blunt-based trailing edge, which has no effect on the supercavitation at higher speeds, but does result in a base ventilated operation at the low speed cruise condition. Therefore, the LUMF model produces less lift and more drag than it would with the flap in the correct position.

TAP-2 WITH FLAP (NSRDC MODEL)

A description of the lift capability for this foil in the 40 to 50 knots speed range can be obtained from Figure 3. The measured lift coefficient decreases with decreasing cavitation number, but there are angles of attack for which the minimum required lift coefficient to support the design load at a given speed is equalled or exceeded. Specifically, $\alpha = 2.8°$ produced a small lift excess over the entire low speed cruise range. There is no question then, that sufficient lift can be generated over the entire low speed cruise range.

Cavitation is a common occurence between 40 and 50 knots, due in part to the excess lift produced by the flap-down condition at these speeds. An additional test would be required to determine if it persists at the lower design loading. Because the upper surface of TAP-2 was designed primarily to avoid separation under the takeoff condition (high C_L), it may be that some shape change would be necessary to eliminate cavitation entirely in this speed range.

The lift-to-drag characteristics of this foil at low speed cruise are summarized in Figure 14, which shows the measured relation between L/D and C_L for three speeds: 40, 45 and 50 knots. The data show a linear relationship between L/D and C_L. A linear least squares regression analysis resulted in the following relation

$$L/D = -0.1 + 27.9\ C_L.$$

Data for the three speeds were plotted with different symbols. For each set, progression from low to high values of L/D corresponds to an increase in angle of attack, typically from $\alpha = -2.2°$ to $\alpha = 2.8°$. In all three cases, the highest measured L/D was obtained at $\alpha = 2.8°$, the highest angle of attack for these runs. The curve may be near its maximum value however (cf. Figure 6) and presumably, still higher angles of attack and values of lift coefficient would not result in a large increase in lift-to-drag ratio.

The lift coefficient also varies with angle of attack. The arrows in Figure 14 indicate operating points (one for each speed) where the lift coefficient is sufficiently high (i.e. provides enough lift to support the design load). For each speed, the angle of attack can be adjusted to give enough lift, which is to be expected since the model is built with the flap in the fully extended position. However, the foil was originally designed to augment its lift by flap control rather than by incidence control. Therefore, it is only with circumspection that L/D values should be read from this graph. A sampling of values is shown below.

V_o knots	C_L	L/D
40	0.38	10.5
45	0.30	8.3
50	0.24	6.6

Lift to drag performance seriously deteriorates as speed increases when incidence control is used.

TAP-2 WITHOUT FLAP

Figures 13 (e) and (f) show L/D ratios for vapor cavitation numbers typical of the low speed cruise range. Since we are interested in the "fully wetted" portion of these curves, ventilation scaling problems do not apply. However, because the flap is missing entirely from the model, the actual operation is in the "base vented" flow regime. σ_v = 0.32 corresponds (for h/c = 1) to a speed of 49 knots and σ_v = 0.34 corresponds to 47 knots. A L/D ratio of 11 was measured for σ_v = 0.32. However, a lift coefficient of 0.30 is required to support the design load at that speed, and the foil ventilates before being able to achieve that C_L by varying the angle of attack when no flap is present. Sufficient lift from the present model could be achieved by an increase in speed, as expected, since this corresponds to a further retraction of the flap on the prototype operation. For example, at σ_v = 0.24, corresponding to 56 knots, where C_L = 0.23 is required. For that condition, fully wetted flow is achieved with α = 1° and a L/D = 9.5 was measured.

It appears that the flapped TAP-2 foil performs best at the low end of the speed range, while the flapless version's performance increases with speed, corresponding to flap retraction of the prototype. How the TAP-2 would perform at low speed cruise in its design configuration with flap control was not measured however.

Today's moderate speed hydrofoil usually has a cruising speed in the neighborhood of 45 knots and is equipped with streamlined foils. The lift-to-drag ratio of such a moderate speed hydrofoil may be greater than 15 when foilborne,[8] although it has been known to drop to as low as 9.5. Based on this consideration, TAP-2's measured performance in the low speed cruise range, using incidence control, would be at the lower end of the state-of-the-art range. How much improvement could be obtained by using the as-designed flap control was not measured.

COMMENTS ON TAP-2 MODEL PERFORMANCE

As shown in Figure 6, TAP-2 performs well at takeoff, with a L/D ratio of 13 at the design lift coefficient. Although the foil experiences a small amount of cavitation, this was not found to significantly affect takeoff performance, due to the small extent of the cavitation.

The performance evaluation is not so well defined in the ventilated regime, meant to simulate the high speed cruise condition, since few data were taken near $\alpha = 2°$, where a transition from fully

wetted to ventilated is observed. This transition is not sharp, and therefore the conditions necessary for ventilation could not be precisely determined. The probable cause has been traced to a design error in the nose, which resulted in the models not carrying the usual separation trigger at that point. This could easily be remedied if further testing was deemed necessary. Data near the transition region are extremely useful since the best ventilated L/D ratios occur there. It is therefore advantageous to operate at an angle of attack slightly larger than what is necessary to maintain ventilation. No precise determination of this angle was made, due to the small number of experimental points.

At one chord submergence, the usual condition for high speed cruising, lift coefficients in excess of the design value of 0.2 have been measured at all tested vapor cavitation numbers for the ventilated condition. Unfortunately, the cavity pressure measurements lacked sufficient accuracy to determine a cavitation number based on cavity pressure. L/D ratios between 7 and 8 were measured near the design point.

Cavity pressures were found to be almost equal to the ambient pressure above the water surface. This has been interpreted as being an indication of full ventilation. In this case, the absence of a pressure drop from surface to cavity suggests that the flow geometry offers little resistance to the passage of air, the foil is said to be fully ventilated. Full ventilation was the rule when TAP-2 was tested at the LUMF. The spray wedges therefore provide an adequate air supply to the cavity.

The medium speed cruise performance, on the other hand, was not measured adequately, due to the fixed flap configuration of the model. When incidence control was used to simulate the performance, low L/D ratios were measured in this speed range.

APPLICABILITY TO PROTOTYPE SCALE

The testing of models can be motivated by two objectives: exploratory research and engineering applications. In the first instance, interest lies primarily in the determination of the governing hydrodynamic properties of the model shape, and there is no immediate intention of referring to a prototype geosim. The bodies thus tested are usually simple in shape, either to conform to some universally tested shape (spheres, discs, flat plates, etc.), which are relatively easy to fabricate or for which mathematical flow models are tractable. The TAP-2 hydrofoil falls in this category. The other category of model tests encompasses the large number of engineering applications in which a model is tested and the results are scaled to some (usually) larger size prototype. In this case, the engineer usually has at least a qualitative knowledge of the model's hydrodynamic behavior, and wants to determine the performance at selected design conditions.

While the primary objective of this project is to ascertain the feasibility of a transition hydrofoil, it is appropriate at this point to comment on the scaling principles with which prototype behavior may be inferred from model tests. While it is understood that TAP-2 is strictly a research foil and that no prototype geosim is intended for any particular craft, it is necessary to be able to predict how a hypothetical larger size foil would behave in the open

seas. This chapter discusses, through examples taken from other hydrofoil tests, data correlations between different facilities. In addition, a brief synopsis of the state-of-the-art in ventilation scaling is given. Recommendations are made for future hydrofoil tests, and for the scaling of data to prototype scale.

Scaling laws are, from the engineering application point of view, just as important as the test data. Whereas geometric similarity is within the test engineer's control, the dynamic similarity scaling relations pertinent to ventilation are still subjects of active research. Such laws would permit us to identify dynamically similar flows on various scales. Appendix B presents a discussion of scaling, with particular attention to ventilated flows.

INVESTIGATION OF FACILITY EFFECTS

Every measurement necessarily involves an unavoidable degree of interaction between the phenomenon being measured and the measuring instrument. The data retain the influence of the measuring instrument. This effect is usually considered undesirable and commonly referred to as measurement error, uncertainty, or resolution limit. While it is possible, in principle, to remove instrumental interference from the measured data, this deconvolution procedure is almost exclusively applied to relatively simple linear systems, and then, only with limited success. For hydrodynamic experiments, the proximity of walls from the model and the ambient turbulence amplitude can affect the measurements.

To increase our confidence in measurements made at different facilities, we shall review data from two geosims: TAP-1 and the BUSHIPS Parent Hydrofoil (BPH) taken at the Langley outdoor tank and at the LUMF. The data reviewed in this chapter have not been previously correlated. In addition to presenting new correlations, this chapter discusses some of the problems of correlating ventilated flows, and makes recommendations on testing methodology.

Wall effects can be minimized by testing in a facility whose dimensions are much larger than the foil. In this fashion, the walls will have little effect on the flow local to the foil. Table 3 compares the dimensions of the foils to those of the facilities in which they were tested. Proximity of the foil to the tank bottom increases the lift, but this effect decreased very rapidly with the foil's height above the bottom. This bottom effect is expected to be negligible for the results reported here.

The proximity of the tank side walls can in principle have a significant influence on flow ventilation from tip vortices. One should guard against the possibility that exaggerated tip cavities, caused by the proximity of the walls, could trigger premature ventilation. From the dimensions given in Table 3 however, there is little likelihood of this being a problem for the data reported here.

There is no guarantee that all flow parameters relevant to ventilation are properly scaled. The degree of air content, wave height, turbulence level, tank mixing and model roughness are suspected of being factors influencing ventilation inception.

TABLE 3
COMPARISON OF FOIL-FACILITY DIMENSIONS FOR
TAP-1, TAP-2 AND THE BUSHIPS PARENT HYDROFOIL TESTED AT
THE LANGLEY HIGH SPEED CARRIAGE AND AT THE LUMF

		TAP-1	TAP-2	BPH
Langley H: High Speed Carriage 1: Tank # 1	depth/chord	5.7 (H)	26.7 (1)	6.4 (H)
	width/span	7.2 (H)	12.8 (1)	6.4 (H)
LUMF	depth/chord	32.0	40.0	36.0
	width/span	13.5	8.0	12.0

Without the benefit of scaling laws, we must make use of visual observations to ensure that the desired degree of ventilation is established. Cavity pressure is an important parameter in that smaller cavity cavitation numbers are associated with full ventilation.

TAP-1 CORRELATION

Data for the TAP-1 hydrofoil are now presented. These data are taken from the work of Holling, Baker and Rood[4] at the Langley facility, and Kramer[7] at the LUMF. Due to the paucity of test conditions, it was necessary to extrapolate the LUMF data to the $\sigma_v = 0.12$ condition prevalent at Langley.

Figures 15 through 19 show the lift and drag coefficients for TAP-1 at Langley and LUMF at two submergences and for two different struts. These figures show that, in the ventilated region, force data agree quite well. This is reasonable since one should expect full ventilation to prevail near an angle of attack of 8.5°, and for the reduced pressures under which the LUMF test was carried out.

Figures 19 through 21 show the effect of varying the ambient pressure on the TAP-1 force coefficients. The data shown here are all for fully ventilated flow. Since both flow conditions and model geometry are approximately alike, the resulting similarity of the measured forces is not a surprise. However, there is a considerable amount of data-scatter in the LUMF data.

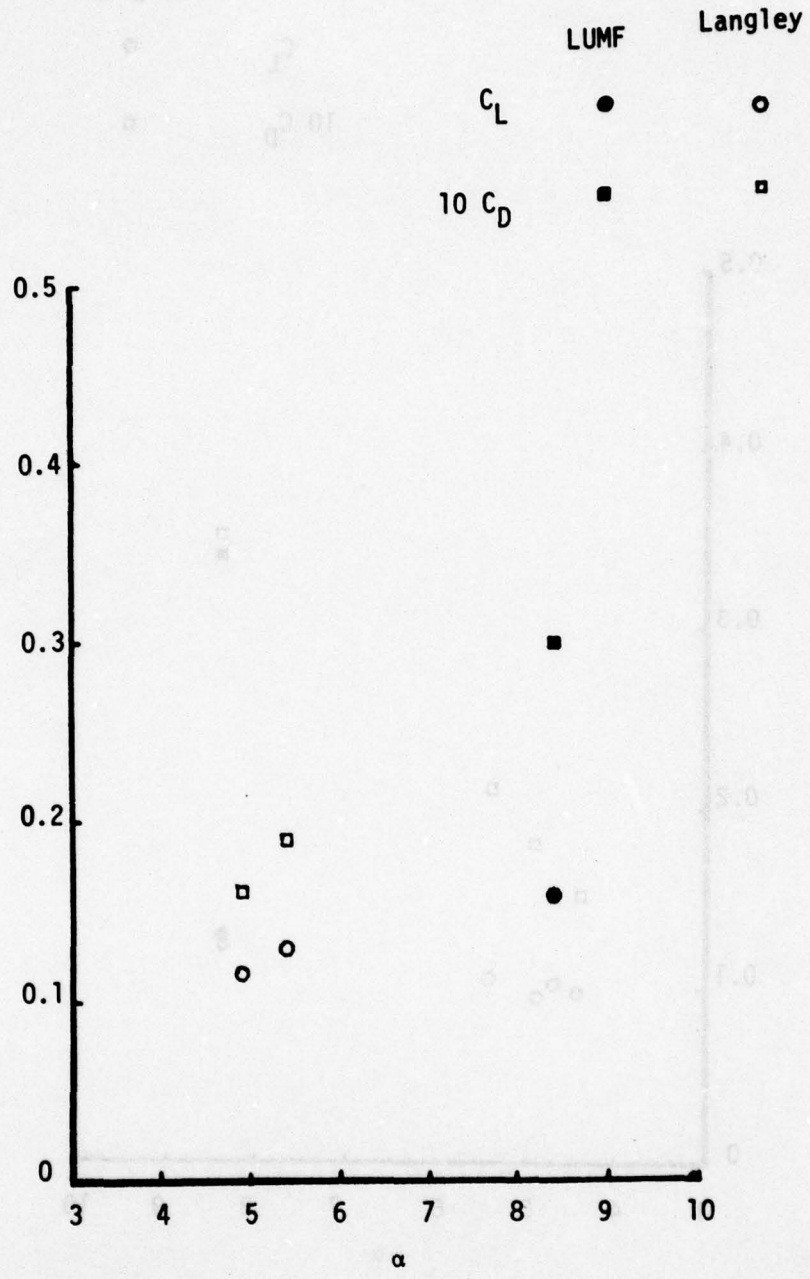

Figure 15 - Comparison of Langley and LUMF Data for TAP-1 at σ_v = 0.12, h/c = 0.5, 12% Strut

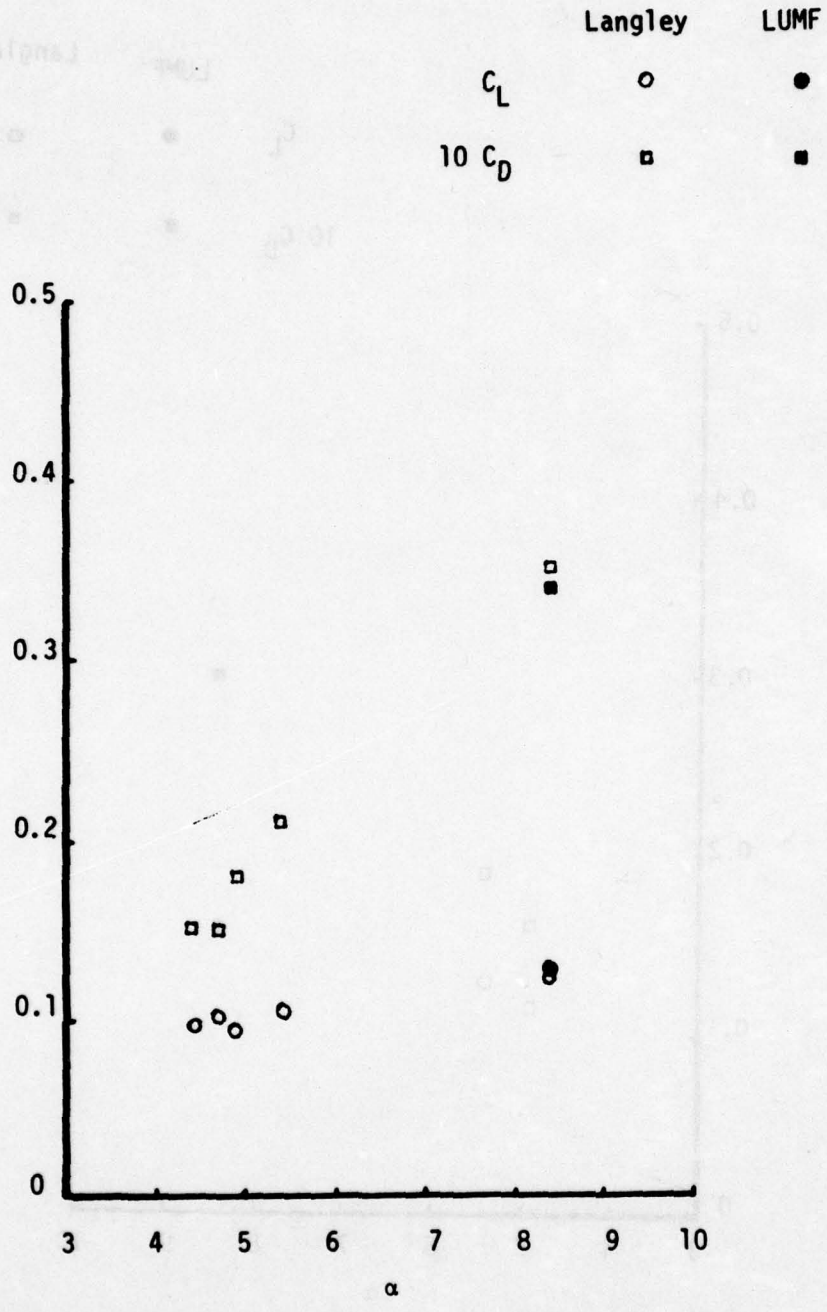

Figure 16 - Comparison of Langley and LUMF Data for TAP-1 at σ_v = 0.12, h/c = 1.0, 12% Strut

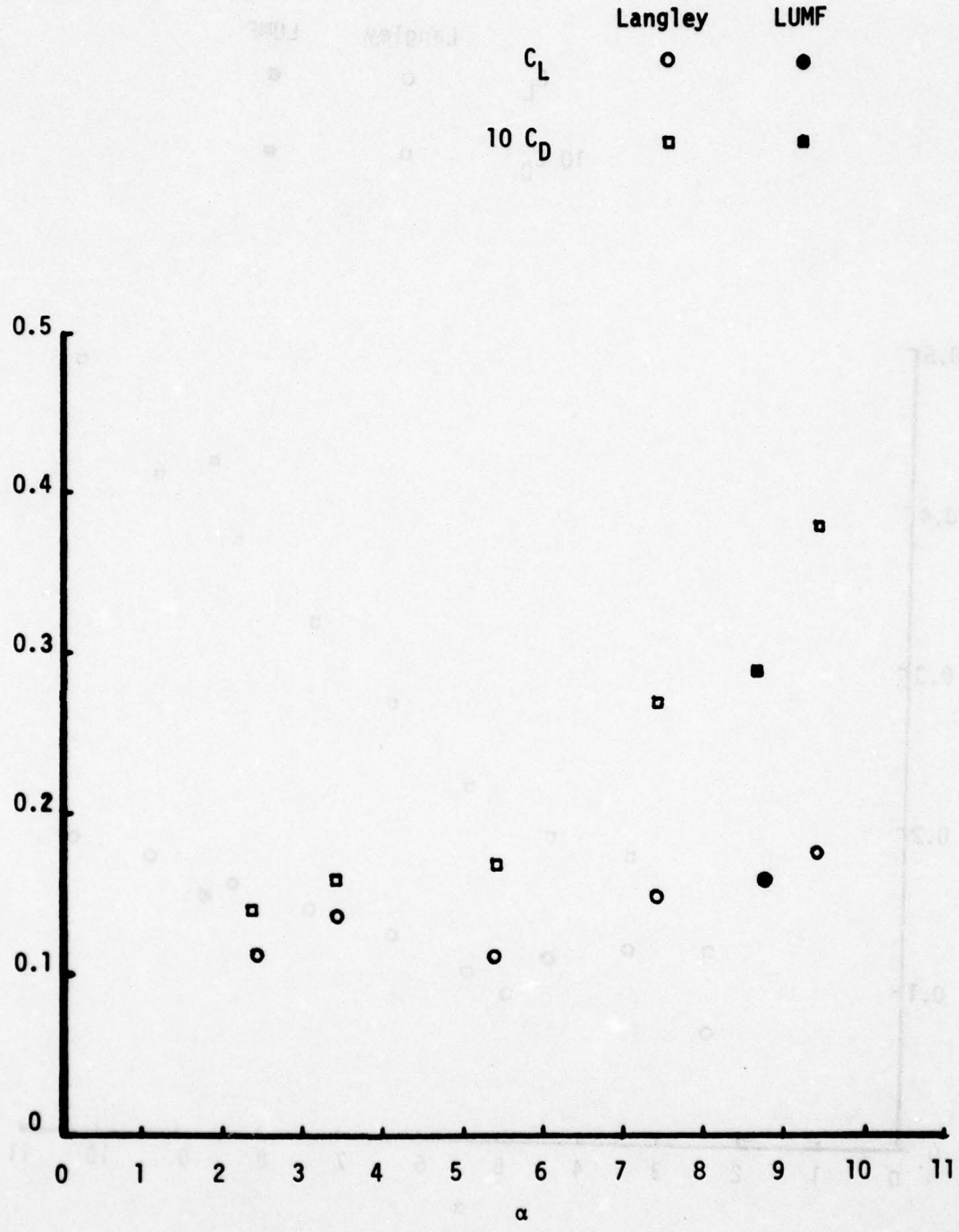

Figure 17 - Comparison of Langley and LUMF Data for TAP-1 at σ_v = 0.12, h/c = 0.5, 18% Strut

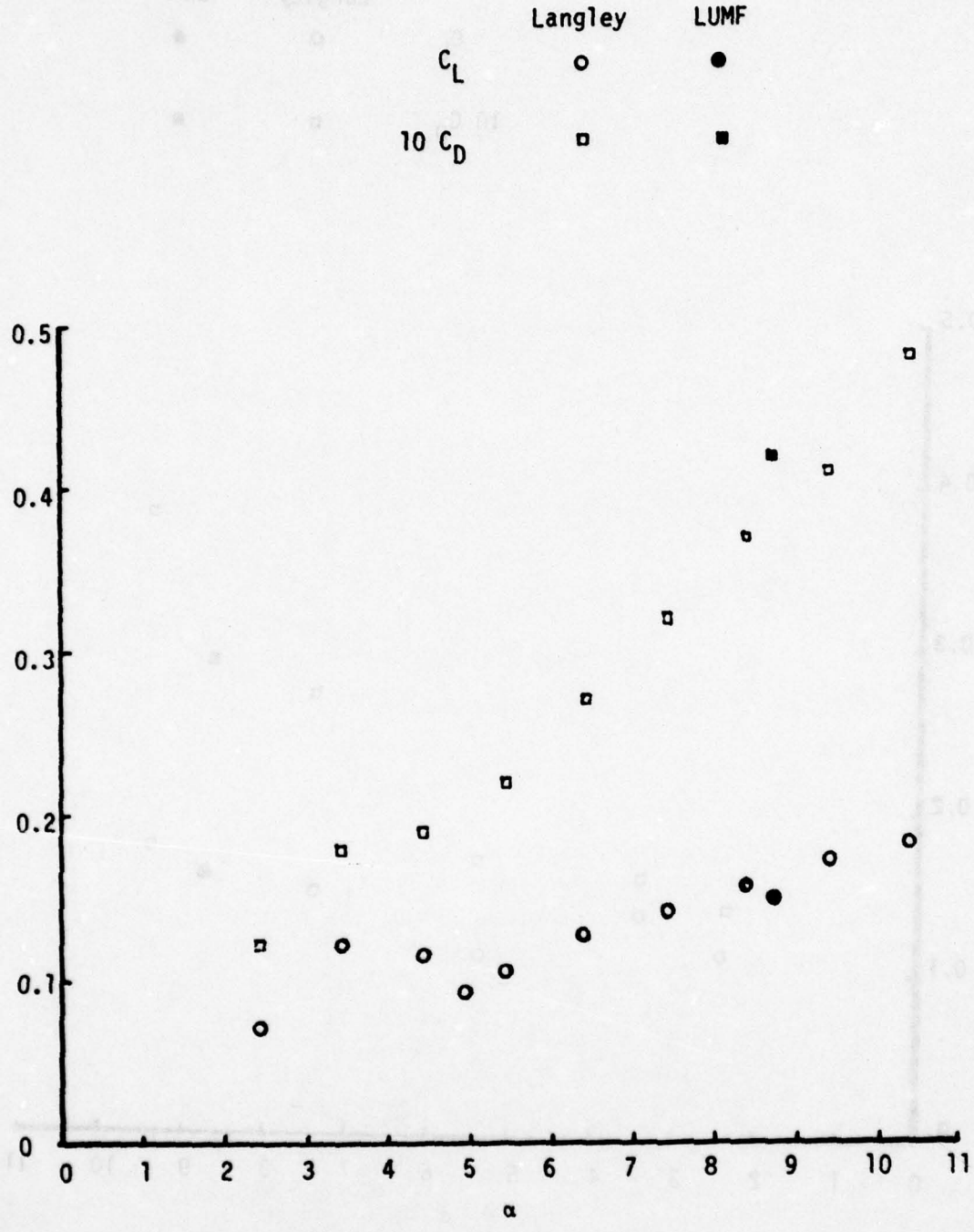

Figure 18 - Comparison of Langley and LUMF Data for TAP-1 at σ_v = 0.12, h/c = 1.0, 18% Strut

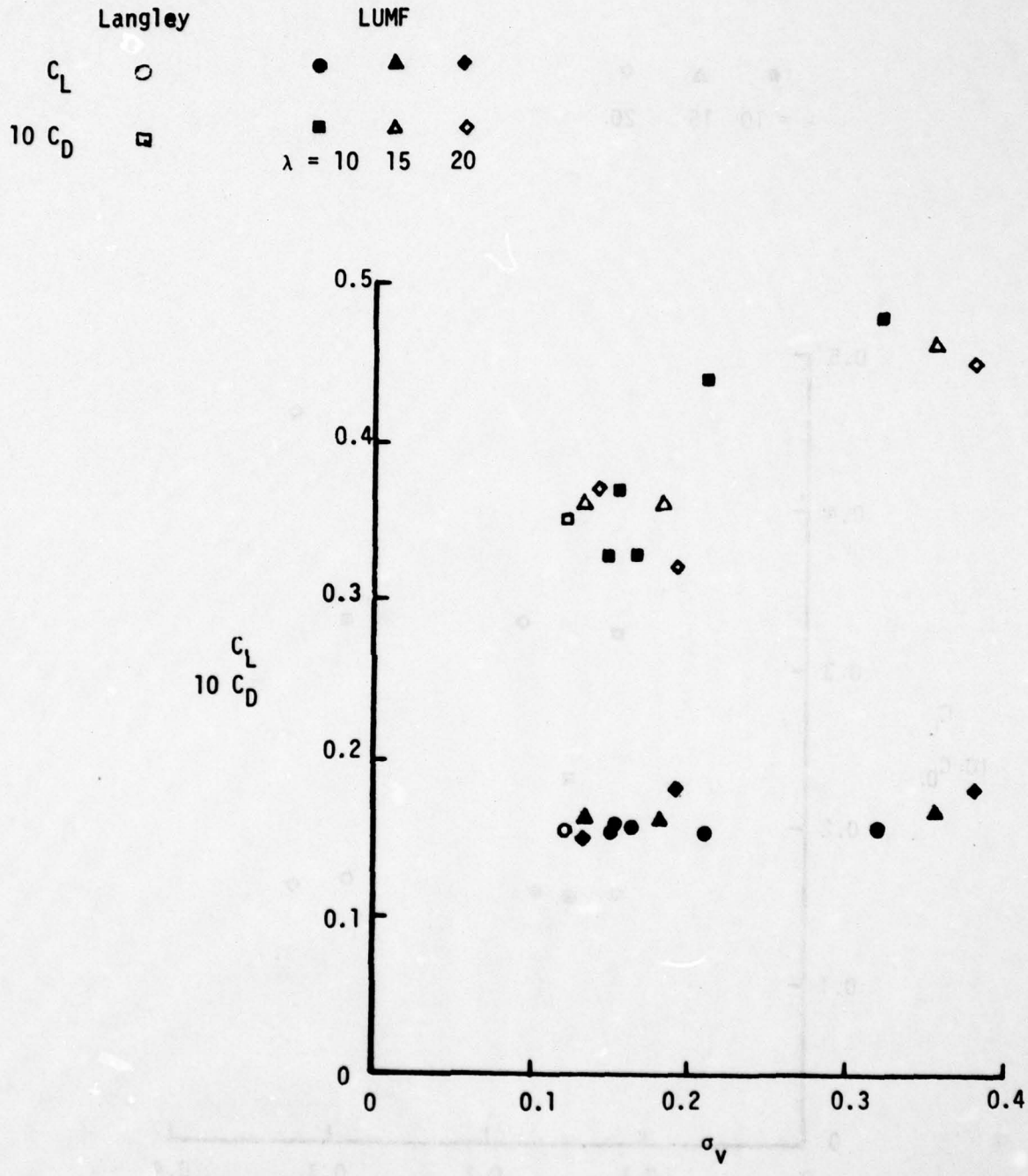

Figure 19 - Effect of Ambient Pressure on TAP-1 Force Coefficients for h/c = 1, α = 8.4°, 12% Strut

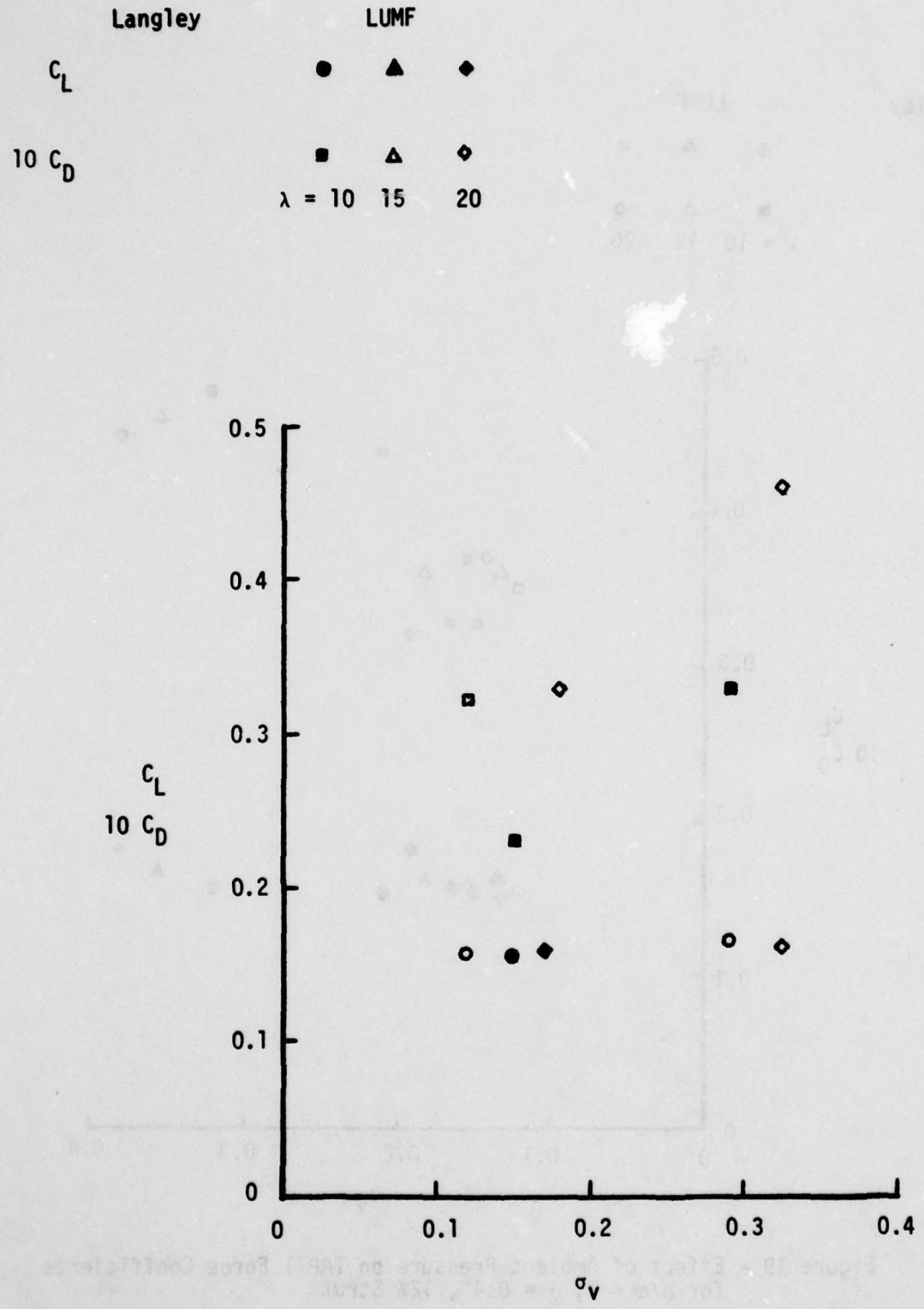

Figure 20 - Effect of Ambient Pressure on TAP-1 Force Coefficients for h/c = 0.5, α = 8.4°, 18% Strut

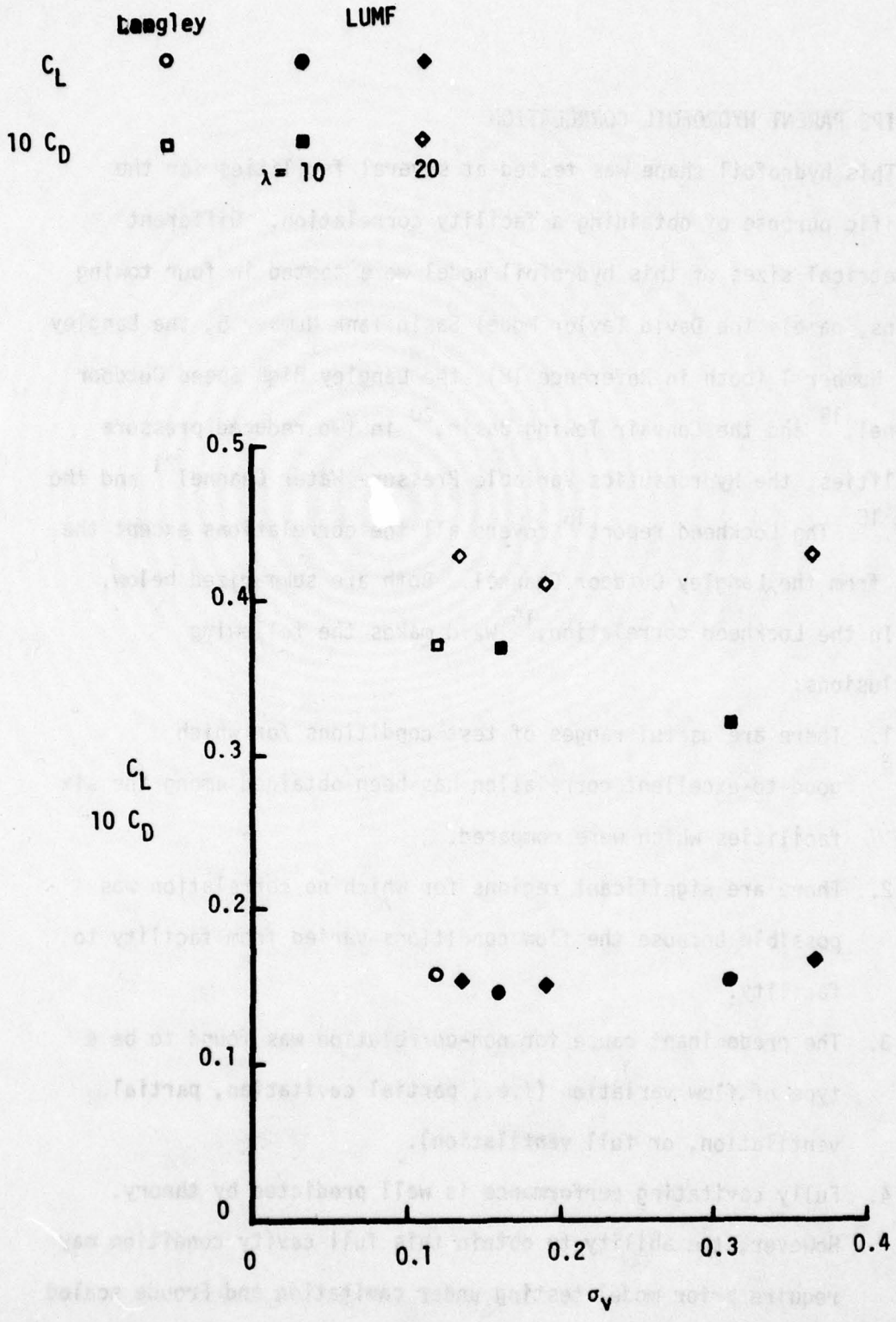

Figure 21 - Effect of Ambient Pressure on TAP-1 Force Coefficients for h/c = 1.0, α = 8.4°, 18% Strut

BUSHIPS PARENT HYDROFOIL CORRELATION

This hydrofoil shape was tested at several facilities for the specific purpose of obtaining a facility correlation. Different geometrical sizes of this hydrofoil model were tested in four towing basins, namely the David Taylor Model Basin Tank Number 5, the Langley Tank Number 1 (both in Reference 18), the Langley High Speed Outdoor Channel,[19] and the Convair Towing Basin,[20] in two reduced pressure facilities, the Hydronautics Variable Pressure Water Channel[21] and the LUMF.[15] The Lockheed report[15] covers all the correlations except the data from the Langley Outdoor Channel. Both are summarized below.

In the Lockheed correlation,[15] Waid makes the following conclusions:

1. There are useful ranges of test conditions for which good-to-excellent correlation has been obtained among the six facilities which were compared.
2. There are significant regions for which no correlation was possible because the flow conditions varied from facility to facility.
3. The predominant cause for non-correlation was found to be a type of flow variation (i.e., partial cavitation, partial ventilation, or full ventilation).
4. Fully cavitating performance is well predicted by theory. However, the ability to obtain this full cavity condition may require prior model testing under cavitation and Froude scaled

conditions. Since partially cavitating conditions require much more analysis before facility correlations can be made, full scale extrapolations are currently without a firm experimental basis.

Similar conclusions can be drawn by reviewing the data of Spangler[19] and Waid.[15] Only in instances when the flow is known to be fully ventilated do the models exhibit similar performance. That is not to say that partially ventilated flows cannot be dynamically similar; it is only for the case of full ventilation that little ambiguity exists about the dynamic similitude of flows. Figure 22 shows a correlation of the Spangler and Waid data for the BUSHIPS Parent Hydrofoil in fully ventilated flow.

COMMENTS ON MODEL-PROTOTYPE SCALING

The conclusions to be drawn from these correlation studies are not novel, but make clear the limitations imposed by our incomplete understanding of the ventilation phenomenon.

First, in instances where the flows were known to be similar (i.e., fully ventilated), identical force coefficients were measured on geometrically similar models. This should not be too surprising for it is a banal restatement of the principle of dynamic similarity. However trite, this finding should be reassuring to the full scale designer.

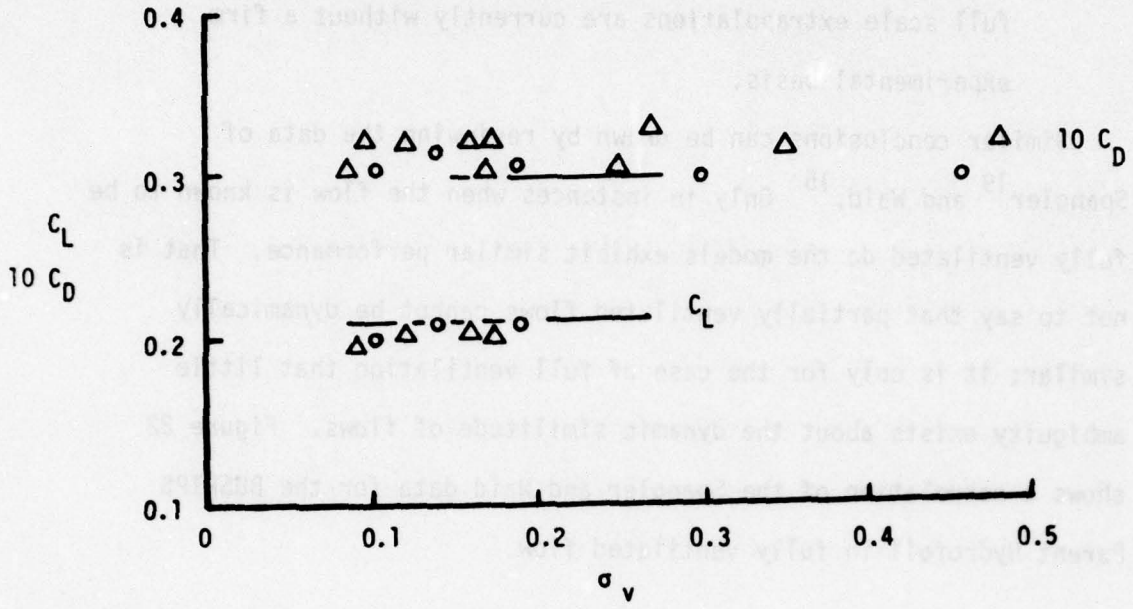

h/c	LUMF	Langley
0.5	o	———
1.0	Δ	

Figure 22 - BUSHIPS Parent Hydrofoil Force Coefficient Correlation $\alpha = 7.4°$, Full Ventilation

Second, full cavity performance is theoretically manageable.

Third, we can only scale performance in flows which are known to be dynamically similar; in practice, this restricts comparisons for the purpose of scaling to fully ventilated flows. The nebulous region called "partially ventilated flow" has not yet been sufficiently charted to permit scaling. In other words, although we may not know precicely how model and prototype become ventilated, we can be certain that forces will scale once full ventilation is established.

Fourth, we must presently rely on the very small amount of knowledge that exists on ventilation inception. It is just as important to be able to predict the conditions under which a foil will become fully ventilated, as it is to have scaling laws for fully ventilated flows. If it is essential to scale model performance for partially ventilated flow, extensive visual observations must be made to ensure that the same cavity exists on the geosims. It is also recommended that cavity pressure be measured.

COMMENTS ON VENTILATION INCEPTION

Very little is known about ventilation inception, or about scaling laws correlating conditions near ventilation inception or partial ventilation. Even now, after twenty five years of investigation, we cannot be sure that what is observed in the laboratory is what takes place at sea.[22] Investigators have simply tried to reproduce the ventilation phenomenon under whatever

laboratory conditions were convenient, and then attempted to extrapolate their conclusions to what they imagined were the actual sea conditions.[23]

Flows suceptible to ventilation exhibit certain common features:

1. a region of separated flow of low net momentum and sub-atmospheric pressure,
2. a surface layer of unseparated flow of relatively high momentum which seals the low pressure separated region from the atmosphere, and
3. a triggering mechanism which allows the atmosphere to breach the surface seal and gain access to the low pressure separated region.

The region of separated flow may consist either of fully wetted separation - usually involving laminar boundary layer separation with turbulent reattachment - or a zone of vapor cavitation. The surface seal prevents atmospheric air from spontaneously invading the separated region. This seal can be extremely thin and still maintain an effective barrier between these two regions of unequal pressures. This is because of the constant atmospheric pressure condition which exists at the free surface. The absence of adverse pressure gradients makes flow at the water surface highly resistant to separation, and the near atmospheric pressure precludes vapor cavities.

The surface seal, maintaining apart two regions of differing pressures, is itself a highly unstable dynamical system. Under the

influence of a sizeable pressure difference, the seal experiences an acceleration, a condition which is known to be destabilizing. This important phenomenon is named after G.I. Taylor,[24] whose research on accelerated surfaces (and other topics) is well known and respected.

These instabilities, triggered by some suitable perturbation, have been proposed as a possible mechanism for ventilation inception.[25-27] The perturbations need not be large. M.C. Eames remarked "In open water, even the smallest ripples appear to be sufficient to initiate ventilation..."[28] Experiments at Leeds University showed that the impact of a single drop of water was sufficient to initiate ventilation.[22]

Assuming that ventilation inception is caused by the growth of Taylor instabilities, we can deduce interesting conclusions concerning the scaling of this phenomenon. Taylor's original analysis[24] can be used as a guide. Assuming the water surface is moving downward with constant acceleration g_1, the surface wave amplitude can be expressed as

$$\eta(x,t) = \eta_0 \cos kx \cosh \zeta t$$

where η_0 is the initial amplitude at time $t = 0$, k is the spatial wavenumber and

$$\zeta = \sqrt{-k\,(g-g_1)}$$

is a factor governing the temporal behavior. Here, g is the gravitational acceleration. Three cases can be distinguished:

$g < g_1$	$g-g_1 < 0$	$\zeta = \sqrt{k \mid gg_1 \mid}$	unstable
$g = g_1$	$g-g_1 = 0$	$\zeta = 0$	neutral

$g > g_1$ $\quad g-g_1 > 0 \quad \zeta = i\sqrt{k\,|\,g-g_1|}$ stable.

The amplification factor in the unstable case is

$$\zeta t = \sqrt{k\,(g_1-g)}\;t$$

Introducing the length scales δ (seal thickness) and c (chord) and the velocity scale V, we can form a time scale ℓ/V so that the amplification factor can be written as

$$\zeta t = \sqrt{\hat{k}\,(\hat{\ell}\sigma_s - \frac{1}{N_{F_{c'}}^2})}$$

where $g_1 = \Delta p/p\delta$ has been expressed in terms of the pressure difference, Δp ($\Delta p = p_o - p_c$), producing this acceleration, and where

$\hat{k} = kc'$ = nondimensional wave number

$\hat{c}' = c'/2\delta$ = nondimensional chord length to seal thickness ratio

$\sigma_s = \dfrac{\Delta p}{\frac{1}{2}\rho V^2}$ = *surface cavitation number*

$N_{F_{c'}} = \dfrac{V}{\sqrt{c'g}}$ = Froude number based on chord length.

On the basis of an analysis similar to the one presented above, Rothblum et al.[26] suggest that the modeling of ventilation inception due to vapor cavitation will entail scaling of the surface cavitation number σ_s, the Froude number based on any model dimension, as well as types of disturbances. Cavity (flow) similarity can be approximately achieved if the cavitation number and chord length Froude number are scaled. The above linear analysis suggest a way of scaling the

disturbances through $\hat{k}$ and $\hat{c}'$. It must be emphasized that the above discussion is based on a linearized analysis and necessarily excludes the possibility of a nonlinear scaling of the surface wave amplitudes.

Figure 23 shows Rothblum's[27] correlation of ventilation inception on surface-piercing struts. Except for the Leeds data, the results are for a series of three strut geosims of different sizes. Each angle of attack should be associated with a different flow condition. Ventilation inception boundaries are plotted as a function of σ and the chord Froude number. Rothblum mentions that this analysis neglects several factors that may be important in the full scale case, for example, viscous effects on the seal boundary layer. Nevertheless, his correlation shown here as Figure 23 presents a strong case for the Taylor instability model.

It is considered advisable, in hydrofoil tests involving ventilation, to introduce a certain amount of roughness on the surface since this produces a cavity which bears closer resemblance to full scale behavior than a smooth model.[31] No scaling of roughness can be proposed at this time. One study[23] reports that the principal effect of roughness is a weakening of the surface seal, possibly by encouraging boundary layer growth, turbulence and vorticity.

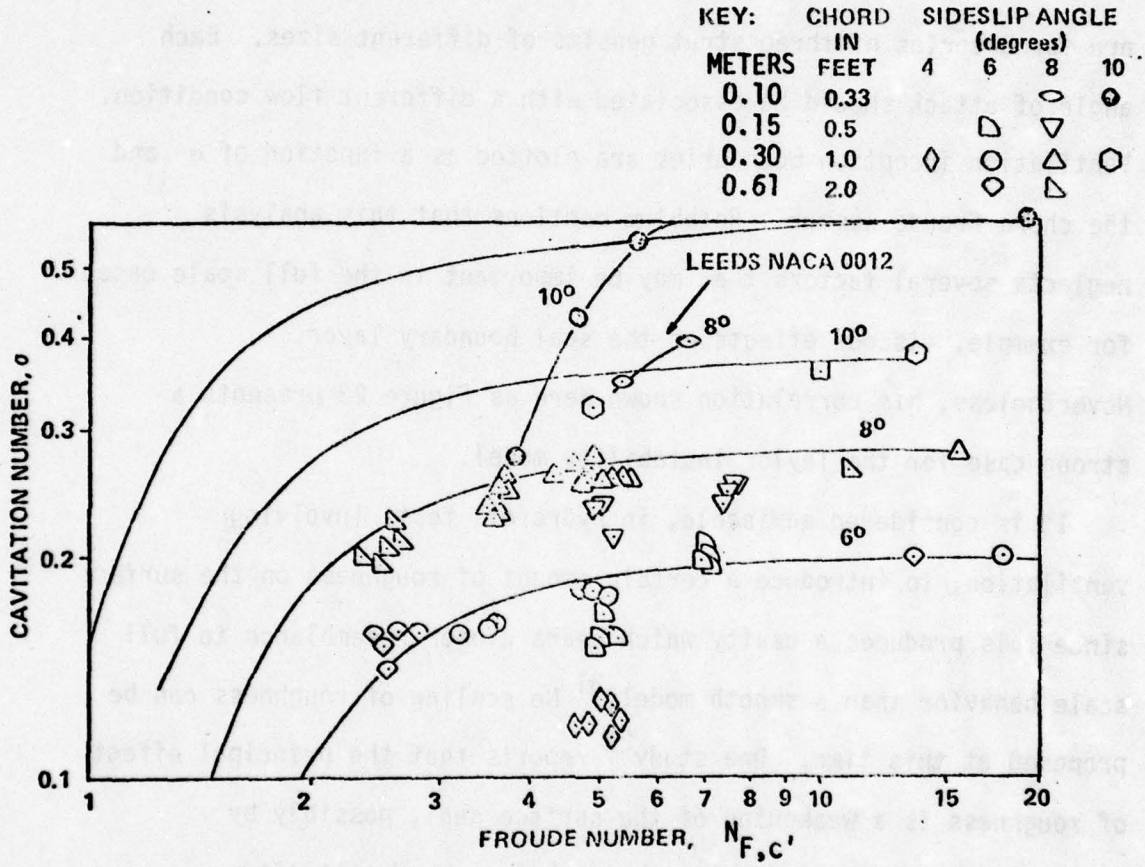

Figure 23 - Ventilation Boundary Correlation for Geometrically Similar Versions of NSRDC Strut Model 2 (Similar to NACA16-021). Also Shown are Boundary Points for NACA 0012 (Data taken from Reference 30 and Rothblum et al.,[29] Waid,[32] and Wright et al.[33]

CONCLUSIONS AND RECOMMENDATIONS

TAP-2 is a variable geometry mixed foil designed to take off fully wetted at 35 knots and cruise fully ventilated at 60 knots. In addition, it was designed to cruise fully wetted in the 40 to 50 knot range, and to have a burst speed capability at 80 knots. To encourage and ensure ventilation, spray wedges are deployed laterally on the strut at high speed, transforming the streamlined shape to a blunt-based one. Two models of this foil system were tested, one at NSRDC and the other at the Lockheed Underwater Missile Facility, a reduced pressure towing tank.

At the design takeoff lift coefficient, $C_L = 0.49$, a measured lift-to-drag ratio of 13.4 was obtained at $\alpha = 2.8°$. This is taken as an indication of good performance. The slight degree of cavitation observed is not believed to be a problem since it is not extensive enough to seriously degrade performance.

Scaled cruise speeds were achieved by testing at reduced pressure with $0.13 \leq \sigma_v \leq 0.34$. Fully wetted flow was observed for $-2° \leq \alpha \leq 1°$ and ventilated flow for $4° \leq \alpha \leq 8°$. The intermediate range $1° \leq \alpha \leq 4°$ was not adequately studied. Data are few for this transition region. The transition from fully wetted to ventilated flow occured gradually and was not well defined. This is thought to be the result of a fabrication defect. A lift-to-drag ratio of 7 is typical for the fully ventilated regime. Cavity pressures close to surface ambient pressures were measured, an indication of full ventilation.

The two models (takeoff model with flap, and cruise model without flap) were tested in conditions chosen to scale the 40-50 knot speed range, but not the operation of the prototype. Using incidence control instead of flap control, L/D values of about 10 were measured, which is at the low end of the state-of-the-art range. Using flap control could be expected to increase this figure, but how much was not measured.

A few recommendations can be made concerning the testing of ventilated hydrofoils. For geosims tested in dynamically similar flows, the force coefficients should be identical. This works well for fully ventilated flows, where we are certain of the flow condition. Our understanding of partially ventilated flows is not yet sufficient to make unambiguous correlations between model and prototype.

Ventilation inception is not fully understood either, but a plausible mechanism has been suggested: the growth of Taylor instabilities on the surface seal. A cursory linear analysis reveals four nondimensional quantities which govern the scaling of this process: the Froude number based on strut chord length, the cavitation number, the seal thickness-to-chord ratio and the nondimensional wave number of the ambient disturbances. Of these, the first two have been successfully used in scaling ventilation inception data. A thorough analytical investigation of this process, taking into account the inevitable nonlinearities, is therefore timely. Such a study is amply justified by the success of available

correlations. The role of wave height in ventilation inception scaling could be investigated, and experiments could be suggested which would determine the predictive accuracy of the theoretical model.

It is also recommended that further experimental work be done to formulate empirical ways of correlating partially ventilated flows.

Experiments should also be performed to determine the effect of seal thickness and disturbance wave number of a ventilation inception. Wave amplitude and model surface roughness should also be considered in model tests. Although it is not known how these parameters scale, they have been observed to affect inception.

ACKNOWLEDGEMENT

The author wishes to thank the following individuals for numerous informative consultations: Mr. Gabor F. Dobay, Dr. Young T. Shen, Mr. Elwyn S. Baker, and Dr. Richard S. Rothblum. The typing and production of this report were managed by Ms. Marjorie Reyes.

APPENDIX A

This appendix lists offsets for the NACA 16-012 strut and the TAP-2 hydrofoil. The strut offsets were obtained from Reference 10 and do not include the ventilation spray wedges described in Figure 2. The foil offsets are adapted from DTNSRDC drawing number E-3265, and do not include the takeoff flap. Each set of offsets is presented in dimensionless form. The strut chord was 0.5 feet (0.152 m) and the foil near chord was 0.375 feet (0.114 m). For the foil upper surface offsets, ℓ denotes the dimensionless distance of the given section from the foil centerline.

x	y
0.000	0.00000
.0125	.01292
.025	.01805
.050	.02509
.075	.03032
.10	.03457
.15	.04135
.20	.04664
.30	.05417
.40	.05855
.50	.06000
.60	.05835
.70	.05269
.80	.04199
.90	.02517
.95	.01415
1.00	.00120

Strut Offsets - NACA 16-012 Basic Thickness Form

Leading Edge Radius = 0.00703

y	z	y	z
0.0000	0.0000	0.00000	0.00000
.00116	.00162	.00109	.00153
.00438	.00298	.00424	.00282
.00993	.00491	.00973	.00471
.01831	.00718	.01804	.00689
.02733	.00978	.02969	.00940
.04613	.01271	.04558	.01227
.06753	.01609	.06687	.01553
.09616	.01996	.09538	.01927
.13496	.02447	.13398	.02362
.20582	.03131	.18778	.02878
.26847	.03696	.24387	.03384
.32467	.04111	.29318	.03753
.35933	.04344	.35751	.04182
.44931	.04873	.39811	.04422
.51053	.05178	.44700	.04684
.59069	.05513	.50784	.04969
.70489	.05862	.58736	.05273
.90222	.06120	.70049	.05578
.95593	.06027	.84000	.05740
1.03649	.05480	.89000	.05660
1.09013	.04840	.96500	.05153
1.17069	.03462	1.01500	.04560
1.22444	.02256	1.09000	.03278
1.28889	.00467	1.14000	.02153
		1.20000	.00502

$\ell = 0.167$ $\ell = 0.50$

TAP-2 Upper Surface

y	z	y	z
0.00000	0.00000	0.00000	0.00000
.00096	.00136	.00071	.00102
.00402	.00264	.00349	.00222
.00940	.00442	.00571	.00296
.01756	.00649	.00858	.00376
.02907	.00887	.01638	.00553
.04478	.01158	.02751	.00758
.06589	.01467	.04280	.00987
.09420	.01822	.06340	.01247
.11187	.02020	.09107	.01542
.17082	.02587	.12858	.01878
.26480	.03360	.16598	.02193
.32038	.03727	.19716	.02413
.35460	.03929	.23520	.02653
.44322	.04378	.28278	.02913
.50333	.04624	.34449	.03191
.58167	.04873	.38318	.03331
.69244	.05091	.42944	.03471
.74667	.05133	.48640	.03591
.79111	.05067	.56000	.03669
.85778	.0462o	.59333	.03616
.90222	.04093	.72667	.02058
.96889	.02953	.76000	.01318
1.01333	.01951	.80000	.00236
1.06667	.00480		

ℓ = 1.00 ℓ = 2.00

TAP-2 Upper Surface

y	z
0.00000	0.00000
.00060	.00084
.00320	.00191
.00531	.00256
.00807	.00322
.01564	.00471
.02653	.00636
.04149	.00820
.06167	.01022
.07424	.01129
.10576	.01360
.13676	.01573
.16218	.01713
.21018	.01936
.22964	.02011
.27582	.02160
.30356	.02231
.33540	.02293
.37251	.02342
.41662	.02369
.46667	.02351
.49444	.02282
.53611	.01991
.56389	.01676
.60556	.01011
.63333	.00438
.66667	.00391

$\ell = 2.50$

TAP-2 Upper Surface

y	z	y	z
0.00000	0.00000	0.00000	-0.00000
.00667	.00251	.01333	-.00500
.02000	.00384	.04000	-.0076/
.03333	.00447	.06667	-.00891
.04667	.00476	.09333	-.00951
.06667	.00484	.13333	-.00967
.10000	.00429	.20000	-.00858
.13333	.00311	.26667	-.00624
.16533	.00191	.33067	-.00384
.20267	.00102	.40533	- .00204
.23467	.00071	.46933	-.00140
.26667	.00078	.53333	-.00153
.29867	.00124	.59733	-.00247
.33600	.00229	.67200	-.00458
.36800	.00364	.73600	-.00727
.40000	.00538	.80000	-.01076
.43200	.00753	.86400	-.01504
.46933	.01056	.93867	-.02111
.50133	.01358	1.00267	-.02718
.53333	.01704	1.06667	-.03407
.56533	.02089	1.13067	-.04178
.60267	.02593	1.20533	- .05184
.63467	.03071	1.26933	-.06140
.66667	.03589	1.33333	-.07176

Tip

Root

TAP-2 Lower Surface

APPENDIX B

THE SCALING OF CAVITY FLOWS

The following analysis is intended as a guide to experimenters who wish to reproduce accurately scaled flows under dynamically similar conditions. For further readings, Birkhoff's monograph[32] is highly recommended.

We shall study the mathematical implications of the equations of fluid mechanics when these equations are subjected to certain transformations. Without actually solving these equations, one can, from a study of their invariance under a specified group of transformations, determine how to obtain dynamically similar solutions. Our analysis rests on the following

PRINCIPLE

If a set of mathematical equations is invariant under a group, then the same is true of all consequences of these equations.

By a group, we mean a set of transformations which contain

i. the identity,

ii. the inverse of any member, and

iii. the product of any two members.

The very general principle that if the hypotheses of a theory are invariant under a group, then so are its conclusions allows us to

determine the group properties of solutions to the equations of fluid dynamics without actually having to integrate them. The elegance and power of this principle is immediately obvious in light of the extreme difficulty of integrating these equations.

The aim of this analysis is not to provide detailed knowledge about hydrodynamical solutions - as indeed it cannot, but to make very general statements about cavity flows.

In Newtonian continuum mechanics, one can make arbitrary changes in the scales of length, mass and time. The invariance of the equations of fluid dynamics under this group of transformations makes possible the

PRINCIPLE OF DYNAMICAL SIMILARITY

Two fluid motions Σ and Σ' are dynamically similar if they can be described by coordinate systems which are related by transformations of space-time-mass of the form

$$x'_i = \chi\, x_i,\quad t' = \tau t,\quad m' = \mu m \qquad (1)$$

where χ, τ, and μ are constants.

In fluid mechanics, a flow is determined by the equations of motion, continuity and state, supplemented by appropriate boundary and initial conditions. To model a certain flow Σ with a scaled flow Σ', one needs to find a particular transformation given by Equation (1) which leaves the flow equations and auxiliary conditions invariant. Note that the character of these equations will impose certain constraints on the scale factors χ, τ and μ. Some freedom in choosing

the scale factors will however remain; this freedom can be exploited by selecting suitably convenient scale factors to define the scaled flow. What is considered "convenient" is left entirely at the discretion of the experimenter, but when a suitable scaled flow has been determined, the experiment can be conducted with Σ', and the behavior of Σ can be found by applying the inverse transformation

$$x_i = x'_i/\chi,\ t = t'/\tau,\ m = m'/\mu. \qquad (2)$$

We note in passing that geometric similarity of all flow boundaries is required by Equation (1) since all linear dimensions are scaled by the factor χ.

The analysis exploits the third property of groups. First, Equations (1) are used to cast the flow equations in dimensionless form by letting χ and τ represent characteristic length and time scales, respectively. These scales, together with physical constants relevant to the flow will appear in the form of dimensionless parameters whose magnitude determine the character of the flow. The flow is invariant under any scaling which preserves the magnitude of these dimensionless numbers. In particular, successive transformations may be found which scale the flow while maintaining dynamic similarity.

We first consider the steady flow of an incompressible, viscous fluid over rigid boundaries. Gravity is also considered. The equation of motion which is applicable to this case is the Navier-Stokes equation

$$(\bar{V} \cdot \nabla)\bar{V} + \frac{1}{\rho}\nabla p + g\hat{i} = \nu \nabla^2 \bar{V} \qquad (3)$$

where $\hat{i}$ is a unit vector in the direction of the gravitational acceleration and ν is the kinematic viscosity. By scaling lengths (χ) and velocities ($\frac{\chi}{\tau} = V_o$) with the transformation in Equation (1), we obtain

$$(\bar{V}' \cdot \nabla')\, \bar{V}' + \nabla' p' + \frac{\hat{i}}{N_F^2} = \frac{1}{N_R} \nabla'^2 \bar{V}' \qquad (4)$$

where

$$p' = p/\rho V_o^2$$

$$N_F = \frac{V_o}{\sqrt{\chi g}} = \text{Froude number,}$$

$$N_R = \frac{V_o \chi}{\nu} = \text{Reynolds number.}$$

The auxiliary conditions, namely continuity

$$\nabla \cdot \bar{V} = 0, \qquad (5)$$

the kinematic boundary condition

$$(\bar{V} \cdot \nabla)\, B_j = 0 \text{ on } B_j = 0 \qquad (6)$$

where $B_j = 0$ is the equation defining the jth rigid boundary, and the no-slip condition

$$\bar{V} = \bar{0} \text{ on } B_j = 0 \qquad (7)$$

are all invariant under the scaling (Equation (1)).

This flow is invariant under the scaling (Equation (1)) provided

i. the pressures are scaled with ρV_o^2,

ii. the scaling be such as to preserve the Froude and Reynolds numbers.

These are (some of) the scaling constraints one would face in order to scale viscous gravitational flow. This result is not new, but does illustrate how familiar scaling laws can be derived from a very general principle.

A cavity introduces an additional boundary condition of the form

$$\tfrac{1}{2}\rho \bar{V} \cdot \bar{V} + \rho g y + p = \text{constant} \qquad (8)$$

where y increases in a direction opposite to the direction of gravity. The constant in Equation (8) is determined by physical conditions at the surface. This boundary condition is essentially an application of Bernoulli's equation on the cavity surface, and on the same streamline, far ahead of the body.

$$\tfrac{1}{2}\rho V_o^2 + p_o + \rho g h = \tfrac{1}{2}\rho V_c^2 + p_c \qquad (9)$$

where p_c is the cavity pressure and V_c is the fluid velocity at the cavity wall. Rearranging gives

$$\frac{p_o + \rho g h - p_c}{\tfrac{1}{2}\rho V_o^2} = \left(\frac{V_c}{V_o}\right)^2 - 1 = \sigma_c, \qquad (10)$$

a general form which reduces to σ_v when $p_c = p_v$.

The importance of the cavitation number can hardly be overemphasized. We have shown how it naturally arises from the surface boundary condition. The significance of this becomes clear when it is realized that the great multitude of (laminar) flows differ only through their auxiliary conditions. One could take the view that due to their very universality, the fundamental laws of Newtonian physics cannot be used to distinguish between different flows. The information about a particular flow resides almost entirely in the

auxiliary conditions which "supplement" the differential formulation of physical laws.

The boundary condition responsible for the presence of the cavity, Equation (9), can be concisely stated by assigning a numerical value to σ_c. The cavity shape is a single-valued function of the cavitation number based on cavity pressure. If cavitation phenomena are to be modeled under dynamic similarity, it is clear then that the appropriate cavitation number must be conserved.

Equation (9) is scale-invariant provided the pressure be scaled with ρV_o^2 and the Froude number be conserved. This should not come as a surprise since Bernoulli's equation is an integral of Euler's equation. If however surface tension were considered, scale invariance would be maintained only with the additional constraint that the Weber number $N_W = \rho \chi V_o^2/T$ (where T is the surface tension) be conserved.

A moment's reflection will show that for ventilated flows, aerodynamic considerations may be important. This is particularly true when the air demand is large, for then the dynamic underpressure caused by the air flow could be appreciable. The cavity is then no longer fully ventilated and the ratio of air to water densities becomes an important scaling parameter. The closure of surface venting behind a blunt-based strut was investigated by Elata,[33] who found that the air flow on the ventilated strut is affected by the ratio of densities of air to water.

Unlike vapor cavitation, which can be modeled by scaling laws which conserve the vapor cavitation number, ventilation introduces the additional involvement of atmospheric air and the resulting aerodynamic consequences. Our search for the appropriate scaling laws should begin, as always, with the physics relevant to the effect in question. In the case of atmospheric ventilation, we have a two-fluid (air and water) problem. In addition to the equations needed to specify the motions of the liquid phase, we need, for a complete description of ventilation, additional equations applicable to the air flow. These additional equations take the usual form of differential equations representing the universal laws of physics, supplemented by the all-important boundary conditions. Not surprisingly, the bulk of information is once again to be found in the dynamic surface condition which, in its most general form, states that in the absence of surface tension, the (normal) stress must be continuous across a fluid interface.

This means that for any point Ω on the cavity surface, the pressure due to the air flow must be balanced by that due to the water flow. Neglecting gravitational effects in the atmosphere, we apply Bernoulli's equation twice: once between point Ω and a point far upstream but on the same streamline,

$$\tfrac{1}{2}\rho_w V_o^2 + \rho_w g h + p_o = \tfrac{1}{2}\rho_w V_c^2 + p_c, \qquad (11)$$

and once between point Ω and the free atmosphere

$$\tfrac{1}{2}\rho_A V_o^2 + p_o = \tfrac{1}{2}\rho_A V_A^2 + p_c \qquad (12)$$

where

ρ_A is the air density,

ρ_w is the water density,

p_c is the cavity pressure,

V_A is the air velocity at point Ω,

V_c is the water velocity at point Ω, and

V_o is the common velocity of air and water far upstream.

Compressibility effects are ignored in Equation (12); this approximation is valid for Mach numbers less than 0.2, and may be overrestrictive in some cases. The importance of ρ_A/ρ_w as a ventilation scaling parameter is, however, independent of compressibility effects.

Eliminating p_c from Equations (11) and (12), we obtain

$$\frac{\rho_A}{\rho_w}\left[1 - \left(\frac{V_A}{V_o}\right)^2\right] = 2\frac{gh}{V_o^2} + \left[1 - \left(\frac{V_c}{V_o}\right)^2\right] \qquad (13)$$

The second term can be identified with a dimensionless cavity pressure coefficient $C_{p,s}$ the third term is simply twice the reciprocal of the depth Froude number squared, and the last term is the negative of the cavity cavitation number. Thus, we obtain the ventilation equation

$$\frac{\rho_A}{\rho_w} C_{p,s} = \frac{2}{N_F^2} - \sigma_c, \qquad (14)$$

relating cavity air pressure (and therefore, air demand) to the hydrodynamic parameters usually associated with ventilation: the

AD-A065 102 DAVID W TAYLOR NAVAL SHIP RESEARCH AND DEVELOPMENT CE--ETC F/G 13/10
PERFORMANCE OF A TAP-2 HYDROFOIL.(U)
JUN 78 P LAFRANCE

UNCLASSIFIED DTNSRDC/SPD-0843-01 NL

2 OF 2
ADA
065102

END
DATE
FILMED
4-79
DDC

cavity cavitation number, and the depth Froude number.

Just as the vapor cavitation number embodies the boundary condition responsible for the presence of a vapor cavity, Equation (14) represents a specification of the ventilated cavity. The cavity shape and pressure are functions of σ_c, N_F and ρ_A/ρ_w. Dynamically similar ventilated flows are those for which the parameters of Equation (14) are conserved.

The importance of preserving ρ_A/ρ_w in scaling dynamically similar ventilated flows cannot be determined by the methods of this analysis. The sensitivity of the flow to this parameter is a matter to be settled experimentally. However, we may infer from the ventilation equation that this parameter plays a significant role when the air demand is large, giving rise to appreciable aerodynamic effects. We remind the reader that compressibility of the air flow at high Mach numbers has been neglected to simplify the analysis.

We note here that the ventilation equation can be expressed in terms of the surface cavitation number

$$\sigma_s = \frac{p_o - p_c}{\frac{1}{2}\rho_w V_o^2} :$$

$$C_{p,s} = -\frac{\rho_w}{\rho_A}\,\sigma_s, \qquad (15)$$

which shows, almost tautologically, that ventilated cavity flow is a function of the difference between cavity and atmospheric pressures.

Since $C_{p,s}$ must by necessity be negative for a cavity to exist, we must have

$$\sigma_c \geq \frac{2}{N_F^2} \tag{16}$$

Conditions for which these two quantities are almost equal correspond to what we know as full ventilation. Increasing differences between these two quantities make $C_{p,s}$ more negative and result in a larger air demand. Since $\rho_w/\rho_A \simeq 773$ at normal atmospheric pressure, an appreciable change in the air demand can result from relatively small variations in σ_c and N_F. The very magnitude of ρ_w/ρ_A should warn experimenters to exercise extreme caution to reproduce σ_c and N_F as accurately as possible, since small errors can easily lead to markedly dissimilar flows. Thus, although the ventilation equation offers hope for the correct modelling of flows which are not fully ventilated, considerable experimental difficulties may be experienced in scaling such flows. Since ρ_A/ρ_w can easily be varied by an order of magnitude (LUMF), this can have a pronounced effect on ventilation.

We are now in a better position to understand the significance of tests performed at reduced atmospheric pressure. The purpose of decreasing this pressure is to achieve small cavitation numbers at relatively low flow speeds. While this procedure is rigorously valid for vapor cavities, it fails to properly scale atmospheric ventilation phenomena. This is because changes in atmospheric pressure necessarily change ρ_A while leaving ρ_w unaffected. The quantity ρ_A/ρ_w is therefore not preserved and dyanmic similitude cannot be achieved.

The failure to model dynamically similar ventilated flows is more severe for cases in which aerodynamics is important, i.e., for incompletely ventilated flows requiring a large air demand. Fully ventilated flows should be reasonably well replicated provided σ_c and N_F be properly adjusted, in view of the magnitude of ρ_w/ρ_A, as previously discussed.

Since the dynamic underpressure caused by the air flow through the cavity is believed to be the mechanism responsible for cavity choking, i.e., surface closure of the cavity, reduced pressure tests should result in larger cavity sizes by delaying cavity closure due to insufficient aerodynamic underpressure. It is therefore more difficult, in a reduced pressure facility, to bring the cavity pressure very much below the ambient atmospheric pressure. This is well documented in Figure 7, where it is shown that the cavity underpressure decreases as the ambient pressure decreases, and explains why fully ventilated flows are "easier to achieve" in reduced pressure facilities. These are all consequences of the reduction in atmospheric density with reduced pressure, and are all manifestations of a failure to dynamically scale the ventilation phenomenon.

Having studied the theoretical basis for the scaling of dyanmically similar ventilated flows, the relative importance of the various scaling parameters remains to be determined. The simplest way to do this is to study the solutions to the equations of fluid motions experimentally.

We have shown that, in the absence of viscosity and surface

tension, the force coefficients must depend the following dimensionless parameters:

$$N_F,\ \sigma_c,\ \rho_A/\rho_w;\ \alpha,\ h/c.$$

Three are necessary for the scaling of gravity, cavity and aerodynamic effects; the last two ensure geometrical similarity. While these parameters model steady, established ventilated flow, they and possibly other quantities may well play different roles in ventilation inception.

On the basis of his correlation of the BUSHIPS Parent Hydrofoil tests, Waid[15] concluded that prototype full cavity flow near σ_c near zero can be inferred from model testing under cavitation and Froude scaled conditions. He also stated that "since partially cavitating conditions require much more analysis before facility correlations can be made, full scale extrapolations are currently without a firm experimental basis."

Thirteen years later, as this report is being written, Waid's conclusion is still valid.

An experiment to accertain the importance of the various scaling parameters would therefore be timely. At least three geometrically similar bodies, for example a "wedge" foil on a strut, could be tested in a reduced pressure facility. Froude number variations could be accomplished by size and velocity scaling, and the cavity cavitation number could be adjusted with changes in pressure. As ρ_A/ρ_w cannot be

conveniently varied in existing facilities,* the purpose of the experiment would be to determine the conditions under which ρ_A/ρ_w (and possibly N_F) can be safely neglected.

---

* See Reference 35 for a ventilation experiment in which density compensation with a heavy gas (Freon) was used to scale ventilation.

REFERENCES

1. Shen, Young T. and Raymond Wermter, "Recent Studies of Struts and Foils for High Speed Hydrofoils," AIAA Paper No. 76-851, presented at the AIAA/SNAME Advanced Marine Vehicle Conference (1976).

2. Baker, Elwyn S., "Notes of the Design of Two Supercavitating Hydrofoils," NSRDC Report No. SPD-479-13 (Jul 1975).

3. Holling, Henry D., "Takeoff Experiments for a Newly Designated High Speed Supercavitating Hydrofoil (TAP-1)," NSRDC Report No. SPD-575-02 (May 1975).

4. Holling, Henry, Elwyn Baker and Edwin Rood, "Experimental Evaluation of the Performance of the TAP-1 Supercavitating Hydrofoil Model at 80 Knots," NSRDC Report No. 4681 (Jul 1975).

5. Baker, Elwyn S., "Design of Hydrofoil Model TAP-2," NSRDC Report No. SPD-575-03 (Jun 1975).

6. Holling, Henry D., "Takeoff Experiments of a High Speed Hydrofoil System (TAP-2)," NSRDC Report No. SPD-575-04 (Jun 1975).

7. Kramer, R.L., "Performance of the NSRDC TAP-1 and TAP-2 Hydrofoil Models," Lockheed Missiles and Space Company, TM 5724-75-46 (May 1975).

8. Wang, D.P. and Young T. Shen, "A Validation Study of the Mixed-Foil Concept for High-Speed Hydrofoils," J. Ship Research, 20, No. 2 (1976) p. 85.

9. Furuya, O., "Nonlinear Calculation of Arbitrarily Shaped Supercavitating Hydrofoils Near a Free Surface," J of Fluid Mechanics, Vol. 68, Part 1, (1975) p. 21-40.

10. Abbott, Ira H. and A.E. von Doenhoff, "Theory of Wing Sections," McGraw-Hill, New York (1949).

11. Nelka, J., "Effect of Mid-Chord Flaps on the Ventilation and Force Characteristics of a Surface Piercing Hydrofoil Strut," NSRDC Report 4508 (Nov 1974).

12. Olson, R.E. and W.F. Brownell, "Facilities and Research Capabilities High Speed Phenomena Division, David Taylor Model Basin, Langley Field, VA," DTMB Report 1809 (Apr 1964).

13. Baker, Elwyn S., "Effects of Cavitation and Ventilation on High Speed Craft Performance," NSRDC Report No. SPD-573-01 (Dec 1974).

14. Baker, Elwyn S., Private communication.

15. Waid, R.L., "Experimental Investigation of the BUSHIPS Parent Hydrofoil Model - Lockheed Underwater Missile Facility," Lockheed Missiles and Space Company Report No. 805568 (Dec 1965).

16. Dobay, G.F. and N.L. Ficken, "Supercavitating and Ventilated Performance of Three Hydrofoil Sections," DTMB Report 1828 (Jan 1964).

17. Ficken, N.L. and G.F. Dobay, "Experimental Determination of the Force on Supercavitating Hydrofoils with Internal Ventilation," DTMB Report 1676 (Jan 1963).

18. Dobay, G.F., "Performance Characteristics of the BUSHIPS Parent Hydrofoil," DTMB Report 2084 (Aug 1965).

19. Spangler, P.K., "Performance and Correlation Studies of the BUSHIPS Parent Hydrofoil at Speeds from 40 to 75 Knots," DTMB Report 2353 (1966).

20. Conolly, A.C., "Experimental Investigation of Supercavitating Hydrofoils with Flaps," General Dynamics Report GDC-63-210 (1963).

21. Scherer, J.O. and J. Auslaender, "Experimental Investigation of 5-Inch Chord Model of the BUSHIPS Parent Supercavitating Hydrofoil," Hydronautics, Inc. Technical Report 343-1 (1964).

22. Swales, P.D. and R.S. Rothblum, "Ventilation and Separation on Surface Piercing Struts and Foils," Dept. of Mechanical Engineering Monograph, Univ. of Leeds, U.K. (1977).

23. Rothblum R.S. et al., "The Effect of Roughness, Wettability and Speed on the Ventilation Characteristics of Surface Piercing Hydrofoil Struts," Dept. of Mechanical Engineering, Preprint, Univ. of Leeds, U.K.

24. Taylor, G.I., "The Instability of Liquid Surfaces when Accelerated in a Direction Perpendicular to their Planes," Proc. Roy. Soc., A201, 192 (1950).

25. Rothblum, R.S., "Scale Effects in Models with Forced or Natural Ventilation Near the Free Water Surface," presented at the 18th Am. Towing Tank Conf., Annapolis (1977).

26. Rothblum, R.S. et al., "Ventilation, Cavitation and Other Characteristics of High Speed Surface Piercing Struts," NSRDC Report 3023 (1969).

27. Rothblum, R.S., "Investigation of Methods of Delaying or Controlling Ventilation on Surface Piercing Struts," Ph.D. Thesis, Univ. of Leeds (1977).

28. Eames, M.C., Commentary on K.L. Wadlin's paper "Mechanics of Ventilation Inception," presented at the Second Symposium on Naval Hydrodynamics, Washington, D.C. (1958).

29. Waid, R.L. "Experimental Investigation of the Ventilation of Vertical Surface-Piercing Struts in the Presence of Cavitation," Lockheed Missiles and Space Company Report LMSC/DO 19597 (1968).

30. McGregor, R.C. et al., "An Examination of the Influence of Waves on the Ventilation of Surface-Piercing Struts," J. Fluid Mech., 61, 85 (1973).

31. Rothblum, R.S., Private communication (1978).

32. Birkhoff, G., "Hydrodynamics," Princeton University Press (1960).

33. Elata, C., "Choking of Strut-Ventilated Foil Cavities," Hydronautics, Inc. Technical Report 605-2 (1967).

34. Schiebe, F.R. and J.M. Wetzel, "Ventilated Cavities on Submerged Three-Dimensional Foils," St. Anthony Falls Hydraulic Laboratory Technical Paper No. 36, Series B (1961).

35. Gilbarg, D. and R.A. Anderson, "Influence of Atmospheric Pressure on the Phenomenon Accompanying the Entry of Spheres into Water," J. Applied Physics, 19, 127 (1948).

DTNSRDC ISSUES THREE TYPES OF REPORTS

1. DTNSRDC REPORTS, A FORMAL SERIES, CONTAIN INFORMATION OF PERMANENT TECHNICAL VALUE. THEY CARRY A CONSECUTIVE NUMERICAL IDENTIFICATION REGARDLESS OF THEIR CLASSIFICATION OR THE ORIGINATING DEPARTMENT.

2. DEPARTMENTAL REPORTS, A SEMIFORMAL SERIES, CONTAIN INFORMATION OF A PRELIMINARY, TEMPORARY, OR PROPRIETARY NATURE OR OF LIMITED INTEREST OR SIGNIFICANCE. THEY CARRY A DEPARTMENTAL ALPHANUMERICAL IDENTIFICATION.

3. TECHNICAL MEMORANDA, AN INFORMAL SERIES, CONTAIN TECHNICAL DOCUMENTATION OF LIMITED USE AND INTEREST. THEY ARE PRIMARILY WORKING PAPERS INTENDED FOR INTERNAL USE. THEY CARRY AN IDENTIFYING NUMBER WHICH INDICATES THEIR TYPE AND THE NUMERICAL CODE OF THE ORIGINATING DEPARTMENT. ANY DISTRIBUTION OUTSIDE DTNSRDC MUST BE APPROVED BY THE HEAD OF THE ORIGINATING DEPARTMENT ON A CASE-BY-CASE BASIS.